Article

Seismically induced soil liquefaction and geological conditions in the city of Jama due to the M7.8 Pedernales earthquake in 2016, NW Ecuador

Diego Aviles-Campoverde[1], Kervin Chunga[2], Eduardo Ortiz-Hernández[2-3], Eduardo Vivas-Espinoza[1], Theofilos Toulkeridis[4], Gabriela Delgado-Morales[1], Dolly Delgado-Toala[5]

[1] Facultad de Ingeniería en Ciencias de la Tierra, Escuela Superior Politécnica del Litoral, Campus Gustavo Galindo Km 30.5 Vía Perimetral, P.O. Box 09-01-5863, Guayaquil, Ecuador. E-mail: daaviles@espol.edu.ec; eevivas@espol.edu.ec; amorales@espol.edu.ec

[2] Departamento de Construcciones Civiles, Facultad de Ciencias Matemáticas, Físicas y Químicas. Universidad Técnica de Manabí, UTM, Av. José María Urbina, Portoviejo 130111, Ecuador. E-mail: kervin.chunga@utm.edu.ec; eduardo.ortiz@utm.edu.ec

[3] Department of Civil Engineering, University of Alicante, 03690 Alicante, Spain

[4] Universidad de las Fuerzas Armadas ESPE, Av. Gral. Rumiñahui s/n, P.O.BOX 171-5-231B, Sangolquí, Ecuador. E-mail: ttoulkeridis@espe.edu.ec

[5] Facultad de ingeniería, Universidad Laica Eloy Alfaro de Manabí, Ciudadela universitaria, vía San Mateo, Manta, Ecuador. E-mail: dolly.delgado@uleam.edu.ec

*Correspondence author: daaviles@espol.edu.ec

Abstract: Seismically induced soil liquefaction was documented after the M 7.8, 2016 Pedernales earthquake. In the city of Jama, the acceleration recorded by soil amplification reached 1.05 g with an intensity of VIII to IXESI07. The current study, integrates geological, geophysical and geotechnical data to build up a geological characterization of the subsoil for the city of Jama in Manabi province in Ecuador. Then the liquefaction potential index (LPI) has been evaluated considering the PGA-rock values calculated from deterministic methods applied to nearby geological faults, as well as the soil acceleration records for the city of Jama since the Pedernales megathrust earthquake. The importance of conducting geotechnical evaluations of a particular colluvial, alluvial and floodplain deposits, for which the liquefaction probability profiles were also obtained, may serve as an useful tool for buildings foundations or earthquake resistant designs. Finally, the site response analysis is presented using a linear equivalent analysis, where previously seismic records compatible with the target spectrum have been selected. Hereby, the results of ground surface effects have been compared with the spectra of the Ecuadorian Regulation of Construction (NEC) in the context of local seismic amplification.

Keywords: Earthquake environmental effects; earthquake-induced liquefaction, site response analysis; Pedernales earthquake; Ecuador.

1. Introduction

There are a variety of geologic effects that may be triggered by strong earthquakes causing severe damages to human settlements as well as strategic infrastructure and even threaten life of inhabitants (Swenson and Beck, 1996; Obermeier, 1996; Egred, 2009; Toulkeridis, 2016; Aguiar and Mieles-Bravo, 2016; Chunga et al., 2017; Moncayo-Theurer et al., 2017; Navas et al., 2018; Cando-Jacome and Martínez-Graña, 2019; Serva, 2019; Vera-Grunauer et at., 2019). Such secondary coseismic effects may include the shaping and modification of a vast area and corresponding landscapes over a longer period of time due to the generation of landslides, ground shacking and slope failure as well as tsunamis amongst many others, which may leave behind zones of destruction and or catastrophic consequences (Giesecke et al., 2004; Michetti et al., 2007; Berzhinskii et al., 2010; Kelson et al., 2012; Wartman et al., 2013; Serva, 2016; Chunga et al., 2018; Xu et al., 2018; Mato and Toulkeridis, 2018; Serey et al., 2019).

Within the earthquake induced geological and geomorphological hazards, the soil liquefaction is the main cause of destruction that is directly related to earthquakes and has the ability for buildings subsidence, position variation or even collapse (Dakshanamurthy, 1973; Obermeier, 1996; CDMG, 1999; Sana and Nath, 2016; Bahadori et al., 2017; Cando-Jacome et al., 2020). Hazen (1919), first proposed one of the main patterns for this coseismic liquefaction phenomenon, while later the physical effects have been evaluated where heavy structures tend to sink and light structures tend to float (Seed and Idriss, 1971; Wang, 1979; Seed, 1985; Wakamatsu, 1992; Obermeier, 1996; Bray & Luque, 2017).

In this context, earthquake environmental effects are the most common expressions registered in thrust earthquakes between 6.9≤M≤7.9 on the central coast of Ecuador (Chunga et al., 2018; Cando et al., 2020). During the earthquakes of 1942 (M 7.9) and 2016 (M 7.8), several liquefaction phenomena that induced processes of lateral spreading in river margins, subsidence, sinkholes and sand boils, were documented in the city of Jama (Mendoza and Dewey, 1984; Swenson and Beck, 1996; Ye et al., 2016; Chunga et al., 2019). Many of these coseismic deformations have been formed in recent soils on floodplains and terraces, where the groundwater is located between 1 and 5.0 meters of depth (Chunga et al., 2018; Salocchi et al., 2020).

Soil liquefaction, is defined as the process of transformation of saturated granular material from a solid to a liquefied state due to the increase in pore pressure, which causes shear stresses and subsequent rupture of the soil skeleton. The sudden action of the seismic load generates an increment in the pore pressure, thus bringing the effective stress to zero, causing a cosismic liquefaction (Youd and Perkins, 1978; Obermeier, 1996; Bahadori and Hasheminezhad, 2016; Bourenane et al., 2018).

General geological conditions of the city of Jama, have the influence of the saturated soils of the Holocene on liquefaction potential analysis, that is, recently deposited sediments such as alluvial, colluvial, paleochannel and paleo-coastal lagoons, which are prone to suffer the phenomenon of liquefaction in seismic area with PGA-soil greater than 0.38 g (Chunga et al., 2019; Salocchi et al., 2020). A map with the delineation of these soils with coseismic potential will contribute to the planning and development of the urban area of Jama.

The current study, presents results of mapping this coseismic geological effects in the surface area of the Pedernales M 7.8 2016 earthquake, and its correlation with the Potential Liquefaction Index (PLI), applying various deterministic methods. This method has started from liquefaction evaluation based on a stress approach proposed by Seed and Idriss (1971). Also, data from Standard Penetration Test (SPT) drilling will be used, which considers corrections for overload effects, water table level and seismic magnitude (Chen and Juang, 2000; Juang et al., 2000; Goharzay et al., 2017).

The variables used to express the liquefaction potential are the demand CSR (Cyclic Stress Ratio) and the resistance CRR (Cyclic Resistance Ratio) with these values, the Safety Factor (SF) may be calculated, using the resistance over demand ratio. If this SF> 1 indicates that this layer or stratum is not liquefiable and SF <1 indicates that it has a high probability that the soil presents liquefaction (Seed and Idriss, 1971). Furthermore, the geotechnical data and the geophysical tests of V_{S30}, Nakamura and downhole tests, allow to build a geological section of the subsoil of the city of Jama, being the interface depth between quaternary soils and tertiary rocks (as to the volcanic basement) at 90 meters depth. Finally, the response of the terrain is going to be modeled using the Linear Equivalent model (analysis of effective stress), from here the response of the soil columns are calculated for each layer (Hashash et al., 2016; Lai et al., 2020).

Prior to on site data collection, information of stratigraphic units and shear-wave velocity are required in order to model the spectra for the city of Jama, this are the soil profiles, and the Ground motion data based in accordance with the NEC-11, 2015, (Norma Ecuatoriana de la Construcción, 2015).

2. Geodynamic settings and description of the study area

In the northwestern edge of South America, the coast of Ecuador has a short record of historical earthquakes. Hence, the importance of studying seismogenic structures of both, subduction and geological faults, in order to estimate the maximum probable levels of seismicity (Egred, 2009; Chunga, 2010). Similar investigations for high seismic potential and PGA-rock faults have been conducted on the southern, central and northern coastal segments of Ecuador (Chunga, 2010; Chunga et al., 2017; 2019; Bejar et al., 2018).

The main seismic source of the Pacific coastline of Ecuador is the subduction interface zone resulting from the Nazca plate grinding under the continental segment formed by the South American and Caribbean plates that occurs at a rate of approximately 47 mm/yr (Pennington, 1981; Hey, 1997; Gutscher et al., 1999; Aguiar et al., 2009; Veloza et al., 2012). The dip variation of the subducting slab, as well as fracture zones of the oceanic crust, define the segments and also their seismic behaviors (Gutscher et al., 1999; White et al., 2003; Chunga, 2010; Chlieh et al., 2014; Nocquet et al., 2016; IOC, 2020).

For the continental coast of Ecuador, four main seismogenic segments have been recognized along the subduction convergent zone (Fig. 1; Table 1; IOC, 2020). The first segment is the southern coast, which includes the Santa Elena Province and the Gulf of Guayaquil with a rupture length estimated of about 200 to 220 km. This corresponds to the coastal zone from

Table 1. Tectonic segments along the coast of Ecuador modified from IOC (2020).

Segment	DEPHT (KM)	DIP (°)	STRIKE (°)	RAKE (°)	WIDTH (KM)	LENGTH (KM)	SLIP (KM/M)	M
GALERA I+II	20	16	30	90	120	560	120/14 100/16.8	8.9
GALERA II	20	16	30	90	120	450	120/6.2 110/7.4 80/9.3	8.6
GALERA I	22	21	27	90	80	110	80/3.4 60/4.5	7.9
ISLA PLATA	15	14	10	90	80	100 /120	2.6	7.8
SALINAS	20	17	5	90	80	200	3.7	8.1

Salango in southern Ecuador up to the offshore area of Guayaquil Gulf, with a maximum estimated magnitude of M 8.1, having a much longer recurrence than the other tectonic segments.

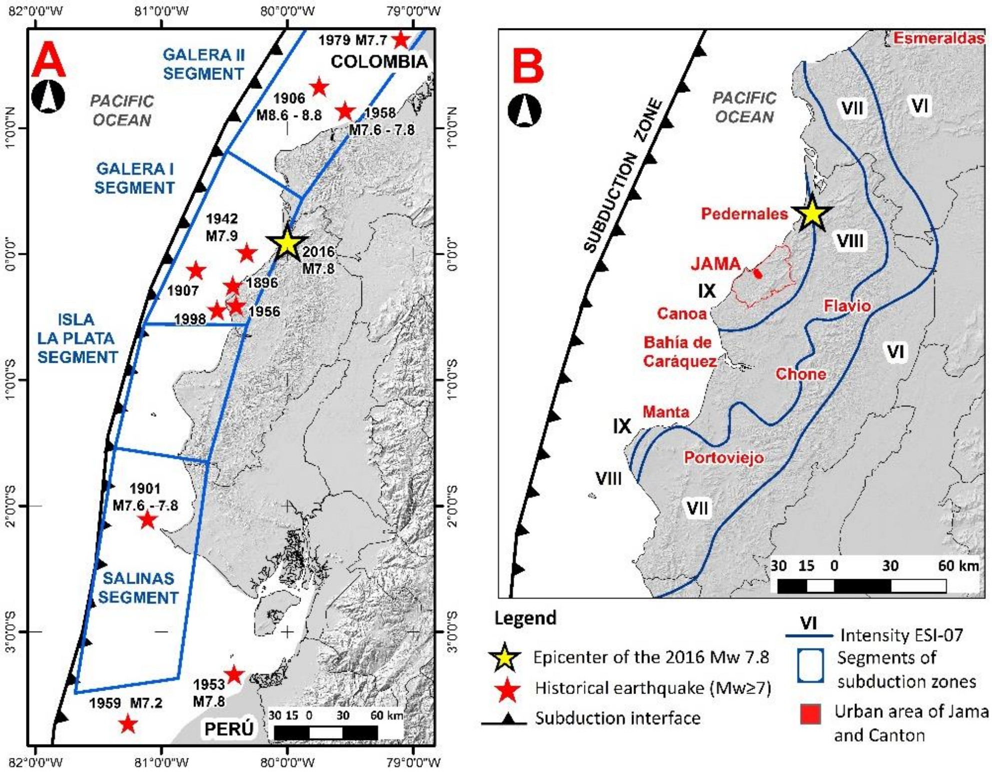

Figure 1. Location maps and seismotectonic setting. A) Regional view of tectonic segments modified from IOC 2020, stars indicate the epicenters of large subduction events occurred in the coastal of Ecuador. B) ESI-2007 macroseismic Intensity of the 2016 Pedernales earthquake (M 7.8).

The second segment is the Isla de La Plata around the Manta peninsula with a rupture area of 100 to 120 km compraising from Bahia de Caráquez to Machalilla, where the estimated magnitude is about M 7.8. This is followed by the third segment in the central coast around the Manabí Province with a rupture area of 110 to 120 km, extending from San Vicente to Muisne.

The maximum magnitude of M 7.9 was documented in Jama in 1942, and the recent M 7.8 Pedernales earthquake in 2016 (Mendoza & Dewey, 1984; Sewnson & Beck, 1996; Ye et al., 2016; Toulkeridis et al., 2017; Chunga et al., 2018). Finally, the fourth segment is located within the northern coast of the Province of Esmeraldas and southern Colombia with a rupture area over 450 km, reaching from the Galera peninsula to the Buenaventura colombian villages, where the maximum estimated magnitude is of about M 8.6 (Chunga et al., 2017; 2018).

Several authors indicate that the third and fourth segments correspond to the same tectonic delineation (see Table 1, Galera I+II), where the maximum magnitude would reach M 8.9 (Kanamori and MacNally, 1982; Yoshimoto et al., 2017; Pulido et al., 2020).

Another morpho-structural feature off the coast of Manabí province is Carnegie, the subduction of this submarine mountain range, with an average thickness of 2.5 km, and has influenced the geodynamics of the coastal zone of Ecuador (Gutscher et al. 1999; Michaud et al., 2009), as well as its coastal geomorphology (Blanco-Chao et al. 2014; Pedoja et al., 2006) and seismogenic characteristics of moderate and high recurrence (Gutscher et al., 1999; White et al., 2003; Graindorge et al. 2004; Font et al. 2013; Chlieh et al. al., 2014; Nocquet et al., 2014; Alvarado et al., 2016; Marcaillou et al., 2016; Collot et al., 2017; Chunga et al, 2019).

The city of Jama is located in the third tectonic segment, where the Jama 1942 (M 7.9) and Pedernales 2016 (M 7.8) earthquakes are the strongest thrust earthquakes recorded during the last 120 years of seismic history (Chunga et al, 2018) (Fig. 1). Other earthquakes of lesser magnitude were documented in the same segment, such as the M 7.1 earthquake of May 3, 1896, followed by the M 7.4 earthquake of June 1, 1907, the earthquake M 7.4 of January 16, 1956 and the earthquake of M 7.1 of August 4, 1998 (Fig. 1). Historical seismicity suggests a recurrence period of 20 years for earthquakes $M > 7.0$, and for larger earthquakes of $M \geq 7.6$ a recurrence between 70 to 80 years (Chunga et al., 2019).

Therefore, the NEC-11 seismic zonation map of Ecuador is comparable with the seismotectonic map of Ecuador, as both classify the coast of Ecuador as an area with high levels of seismicity associated with interplate earthquakes, indicating rock acceleration values between 0.45 and 0.55 g (Chunga, 2010; NEC-11, 2015). Due to its proximity to the subduction zone, the city of Jama is located in the province of Manabí within the central coast of continental Ecuador, whose territory is referred to the highest seismic zone with PGA-rock of ≥0.5 g (Nec-11, 2015).

The recent Pedernales earthquake reported in 2016, registered for the city of Jama a PGA-soil in the order of 1.0 to 1.05 g, while for the site of the epicenter in Pedernales a PGA-soil of 1.4 g was registered (IGEPN). Referring to the strongest aftershocks affecting the city of Jama, the most significant ones were registered on May 18, 2016 with M 6.7 and M 6.9 (Toulkeridis et al., 2017; Beauvalet al., 2018; Chunga et al., 2018). These seismic sequences helped to established that earthquakes from M 6.9 can generate a liquefaction phenomenon in saturated soils where the water table is less than 10 m (Chunga et al., 2018).

The second seismic source is represented by geological faults. In the current study, the seismic parameters of the faults have been consulted from the geometric parameters for each of the selected faults, including: (1) the spatial projection of the fault length on the ground, (2) type and kinematics of the fault, (3) the structural immersion and estimated angle of the fault displacement "in focal mechanism analysis", and (4) the width of the seismogenic structure. With these parameters and applying the equations most adaptable to the tectonics of the region, the magnitude, macroseismic intensity and acceleration (PGA-Rock, Peak Ground Acceleration-horizontal) have been determined. Segmented faults have a lower magnitude, therefore the slip rate of the fault requires many smaller earthquakes in order to accommodate a cumulative seismic moment (Well & Coppersmith, 1994; Wesnousky, 2008; Stirling et al., 2013; Chunga et al. al., 2019).

The current study covers an area of 579 km^2, considered to be deterministic for seismic hazard on the entire canton of Jama. Meanwhile, the detailed geological analysis and geodynamic conditions of the subsoil is conducted over the urban area of Jama with a total of 2.48 km^2. The Jama canton has 20,230 inhabitants and represents 1.7% of the total population of the province of Manabi, with an annual growth of 6.4% (INEC, 2010; Stay-Coello, 2018). The cantonal capital is the city of Jama with 4,719 inhabitants. Most of their houses are built in low lands of alluvial plains and abandoned terraces of floodplain. The altitudes are between 5 to 10 m.a.s.l. The highest reliefs do not exceed 25 m in altitude, being located southeast of the urban area.

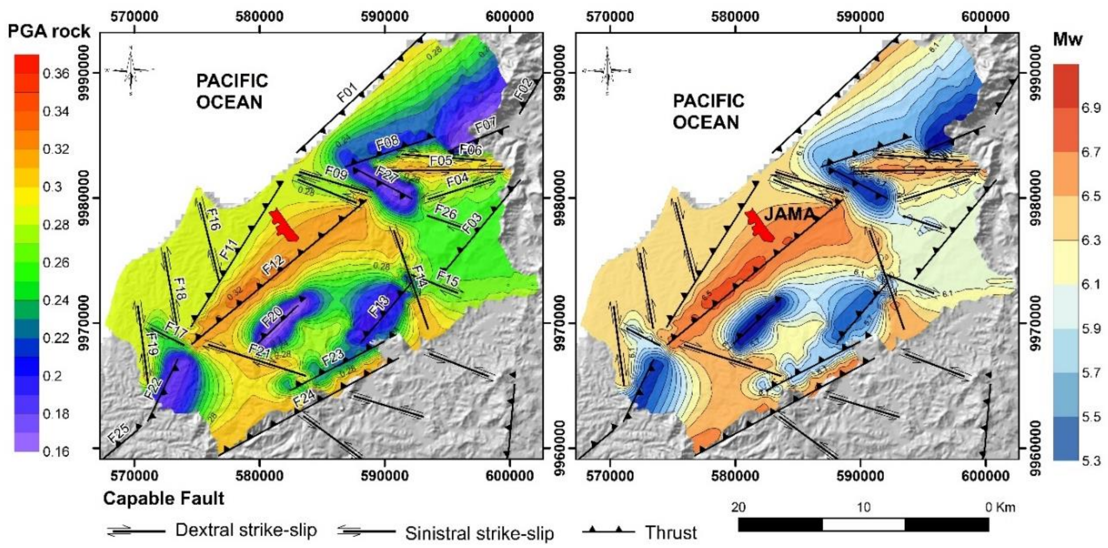

Figure 2. Map of maximum magnitudes and PGA-Rock obtained from the analysis of capable geological faults in the Jama canton.

3. Data and Methodology

Contributing to the understanding of the seismic hazard of Jama, a geological faults catalog has been prepared including 27 active segments capable of generating moderated earthquakes of 5.3 to 6.5 of magnitude (M) and PGA-Rock in the order of 0.17g to 0.32g. The faults are abbreviated from F01 to F27, as shown in table 2. The larger F01, F12 and F24, are classified as reverse faults, having between 16 and 18 km long. This faults are proneto generate earthquakes between 6.4 and 6.5 with a PGA-h of 0.30g to 0.32g. Seismicity levels of M 6.2 and M 6.3 are associated with shear-type faults (F06, F09, F16, F18 and F19), with lengths ranging between 5.7 to 6.8 km, and the accelerations in rock are in the order of 0.29g.

In this context, the city of Jama is predisposed to two types of seismic sources, being large subduction earthquakes with regional coseismic effects, and local moderated earthquakes associated with the activation of geological faults. Hereby, local earthqueakes can reach magnitudes between 6 to 6.9 and, strong earthquakes with magnitudes between 7 to 7.9. For the city of Jama, an acceleration in rock of 0.5 g is determined, which may be amplified in soils reaching values as high as 1.05g, as estimated for the 2016 Pedernales earthquake (Chunga et al., 2019). Table 2, also includes the maximum magnitudes determined by fault directly affecting the city of Jama.

Evaluating the liquefaction potential and the earthquake site response in the city of Jama includes three distinctive stages:

(i) Field reconnaissance and outlining of Quaternary lithological units of the urban area, and their relationship with the field borehole. In-situ testing and laboratory experiments, leads up to the construction of a stratigraphic profile of the subsoil up to -45 m deep and determine the basement depth in Jama urban area using active seismic methods (Geotechnical and geophysical data available from Chunga, 2019 and Daza et al., 2019).

(ii) Evaluation of the liquefaction potential index (LPI) through deterministic risk-based methods from SPT-based simplified procedure and shear wave velocity measurements, taking into consideration a seismic hazard scenario calculated for a return period of 475 years which is amax = 0.5 g. This technique aids in the identification of the depth of the maximum deformations induced by liquefaction. The approach proposed for the evaluation of the liquefaction potential index of soil units is based on results obtained from laboratory tests, based on the grain-size characteristics and Atterberg limits of the soil, considering geotechnical parameters proposed by several previous studies (Wang, 1979; Seed et al., 1985; Chen and Juang, 2000).

(iii) Determination of the geometric mean spectra in rock and soil using an one-dimensional model in Deepsoil program, and compared with the Seismic spectra of the NEC-11 (2015), for Jama D and E geotechnical soil profile types. Using the shear wave velocity values for the underlaying strata, the rock profile was found to be categorized under C profile using the NEC (2015), this means the soil has bad quality considered to be dense soil or soft rock making it prone to have considerable side effects in case of an earthquake, so that the quality of the filtering is adjusted to the target spectrum, geotechnical parameters typical of the study scenarios were also entered into the PEER Ground Motion Database (Earthquake records from PEER NGA strong motion database, https://ngawest2.berkeley.edu/).

Table 2. Geological Faults Catalog for the Jama canton.

Fault	*Mechanism*	*Fault length (km)*	*Fault depth (km)*	*Dip-direction fault*	*Rake*	*Fault width (km)*	*Estimated Magnitude M*	*Levels of reliability*	*PGA-Rock (g) **
F01	Reverse	16.3	12	140	90	8	6.39	deducible	0.30
F02	Reverse	5.5	12	310	90	6	5.50	deducible	0.19
F03	Reverse	10.3	12	330	90	7	6.01	true	0.25
F04	Shear fault Sx	5.0	12	-	-5	6	6.17	deducible	0.27
F05	Shear fault Sx	10.0	12	-	-5	7	6.43	true	0.31
F06	Shear fault Dx	6.8	12	-	-175	6	6.28	deducible	0.29
F07	Reverse	4.8	12	125	90	5	5.39	deducible	0.17
F08	Reverse	7.6	12	335	90	6	5.77	true	0.22
F09	Shear fault Dx	5.7	12	-	-175	6	6.22	deducible	0.28
F10	Shear fault Sx	5.0	12	-	-5	6	6.17	deducible	0.27
F11	Reverse	13.7	12	305	90	7	6.25	true	0.29
F12	Reverse	18.2	12	325	90	8	6.48	deducible	0.32
F13	Reverse	6.3	12	322	90	6	5.61	deducible	0.20
F14	Shear fault Dx	8.4	12	-	-175	6	6.36	deducible	0.30
F15	Shear fault Dx	4.0	12	-	-175	5	6.08	deducible	0.26
F16	Shear fault Dx	6.5	12	-	-175	6	6.27	deducible	0.29
F17	Shear fault Dx	3.0	12	-	-175	5	5.98	true	0.25
F18	Shear fault Sx	6.1	12	-	-5	6	6.24	true	0.28
F19	Shear fault Dx	6.3	12	-	-175	6	6.26	deducible	0.29
F20	Reverse	4.5	12	328	90	5	5.34	deducible	0.17
F21	Shear fault Dx	8.2	12	-	-175	6	6.36	deducible	0.30
F22	Reverse	5.6	12	153	90	6	5.52	true	0.19
F23	Reverse	8.5	12	338	90	6	5.86	true	0.23
F24	Reverse	16.4	12	335	90	8	6.39	true	0.31
F25	Reverse	4.8	12	330	90	5	5.39	deducible	0.17
F26	Shear fault Dx	3.2	12	-	-175	5	6.00	true	0.25
F27	Reverse	5.3	12	203	90	6	5.47	deducible	0.18

*Values determined based on Fukushima & Tanaka (1990) * equations.*

For the delineation of the faults in Jama, the geomorphological features, direction and intersection of the hill reliefs have been considered, that enable us to aproximate the dimension of the faults without oversizing the length of these seismogenic structures. The tectonic activity was associated to similar earthquakes of the upper plate geological faults with hypocentral distances less than 15 km (Santibáñez et al., 2019).

The equations of Wells and Coppermish (1994), used in the analysis of seismic hazard for the upper plate geological fault, is as follows:

Estimated magnitude (M) = 5.08+1.16*LOG (Lf) (1)

Fault displacement (in meters) = EXP (-1.38+1.02*LOG (Lf)) (2)

Where Lf is the length of the capable geological fault.

We consider the equations proposed by Wesnosuky (2008) and Leonard (2010), these defines that a fault of the same length may have different magnitudes depending on the type of faults, being inverse, normal or shear. The spatial delineation of the faults were developed on GIS platform as shown in Figure 2. Wesnousky (2008), proposes modifications and corrections to the previous formula to estimate maximum magnitudes, such as:

Strike-slip faults: M = 5.56 + 0.87*Log (Lf) (3)

Normal faults: M = 6.12 + 0.47*Log (Lf) (4)

Reverse faults: M = 4.11 + 1.88*Log (Lf) (5)

In equations 3-5, Lf is the capable fault length.

These regression equations indicates, that not all types of faults of the same dimension are able to generate earthquakes of the same degree of magnitude (Stirling et al., 2013; Wesnousky, 2008; Chunga, 2010). This concept is applied in the faults delineated for Jama, considering that those faults are inverse and are potentially capable of generating earthquakes greater than others of the same length, but with different tectonic stresses such as shears and traction.

Furthermore, the values of the Peak Ground Acceleration (PGA-Rock) using the equation proposed by Fukushima and Tanaka (1990) has been estimated.

PGA rock = (10^(0.41*M-Log10(Hf+0.032*10^(0.41*M))-0.0034*Hf+1.3))/980 (6)

In equation 6, Hf is the depth of fault and M the estimated magnitude.

The data obtained from magnitudes and PGA-rock have been interpolated using the ArcMap GIS and Surfer programs, applying the “gridding” method generating iso-value maps, while PGA data interpolations in rock are showed in Figure 2.

4. Geomorphological conditions and Earthquake-induced environmental effects

The Jama urban area has six well-delineated geomorphological features in the terrain such as: intertidal flat, alluvial plain, ancient floodplain, colluvial, abandoned floodplain and soft rocks. The soft rocks are composed of siltstones and claystones, from the Onzole and Borbon formations, in addition to other outcrops from the Punta Blanca, Tosagua, Dos Bocas, Villingota, Angostura formations, and some recently identified quaternary deposits. Their ages range from the Oligocene to the Pliocene, covered by unconsolidated sediments from the Pleistocene to the Holocene.

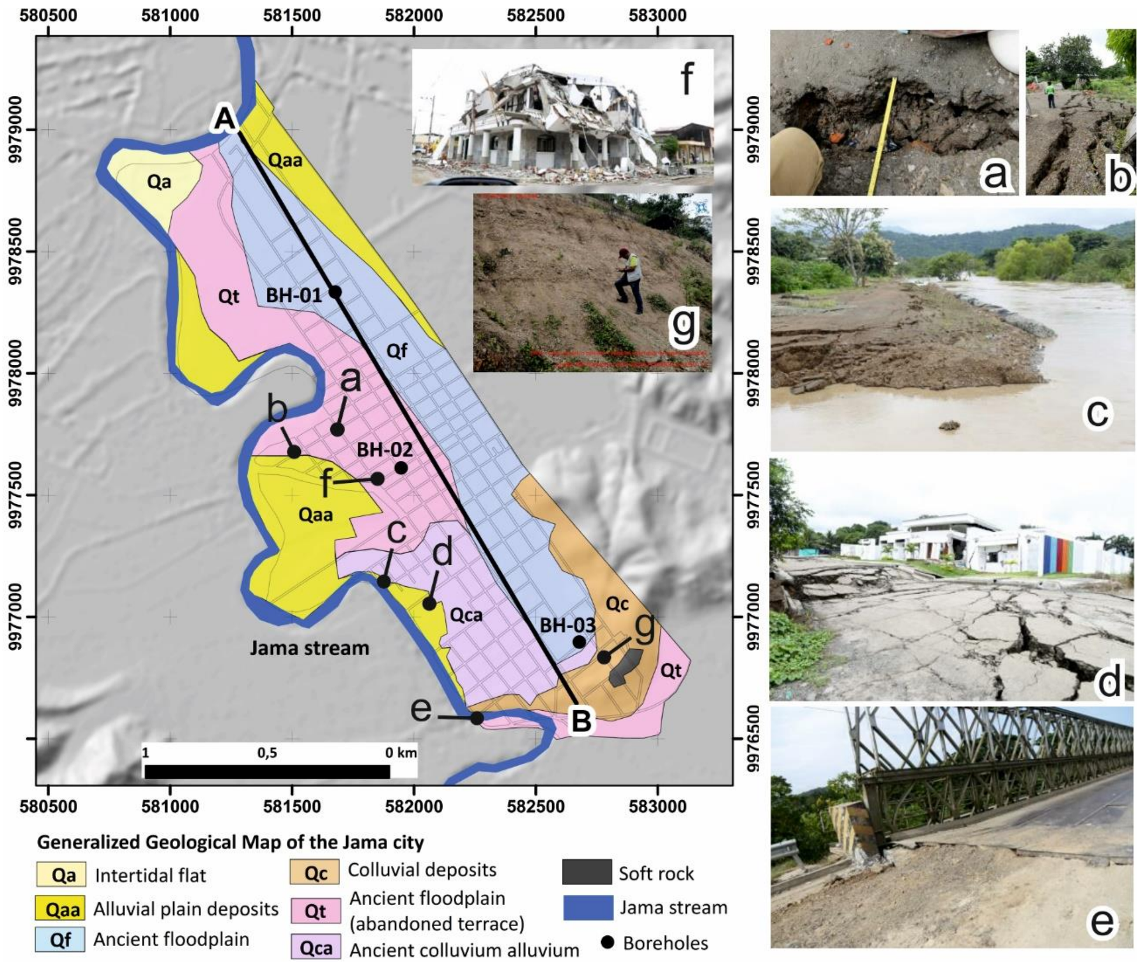

Figure 3. Geological map of the urban area of Jama city and earthquake environmental effects documented few days after the M 7.8 2016 earthquake

Description: a) soil cracks on soil 120 m long and 38 cm wide, VIIIESI-07 intensity; b) lateral spreading on filled sector on river side, VIIIESI-07 intensity; c) lateral spreading in river bank, soil cracks in natural soil 20 to 25 cm wide, VIIESI-07 intensity; d) ground deformation and subsidence, severe damage to the structure Sol de Oro (Economical and Social Inclusion Ministery), assigned IXESI-07 intensity; e) Ground subsidence above bridge anchorage, vertical uplift of 10 cm, VIIIESI-07 intensity; f) building damage due liquefaction, flaws in the structural design of the building and the por quality of the construction, VIIIESI-07 intensity; and g) debris and rocks falls, VIIESI-07 intensity.

In the road cut of several hill slopes, the stratigraphic sequence of the colluvial soils with angular fragments of highly altered claystones is evidenced, interspersed at some levels by layers of distal rain triggered lahars. The height of the slope reaches between 15 to 20 m. In the terraced areas, on the upper level there are sandy loamy soils, which are not very compact having desiccation cracks, there are some areas with less depressions and being flooded demonstrating anthropogenic subsidence (BH-03 in Fig. 3). At the lower level, sandy soils of medium granulometry, somewhat silty, limit the floodplain soils of alluvial plains. In the riverbanks of the

Jama River, appear in the alluvial plain areas silt layers with few intercalations of very fine sand, having moderate to high plasticity.

During the Pedernales earthquake of April 16, 2016, cracks in loose soil with a thickness of up to 20 cm are evidenced in the alluvial terrace area, while in other areas of the transitional limits of alluvial plain and terrace were reported lateral displacements with cracks that reached a 30 cm opening in loose soil. One of the most significant damages was the collapse of the CIBV, a children nursery, located on sandy silty soils in alluvial plain, where soils liquefaction and cracks of up to 25 cm opening in loose soils, considerably deformed the access roads (Fig 3d).

Shrimp farms and their transition to the alluvial plain, where these types of unstable soils presented soil liquefaction and lateral displacements, occupy the intertidal flats to the north of the urban area (Fig. 3). The areas most prone to coseismic deformations in the terrain are intertidal, alluvial plains and ancient floodplain. Mixed construction and reinforced concrete buildings had partial and total damage, both located in areas of lower alluvial terrace in the urban area of Jama (Fig. 3f).

In the lateral steps of the bridge over the river Jama, vertical displacements of the metal and concrete structure were evidenced, where the streets were filled with stone materials in order to gain access to the town of Pedernales, due to the emergency of the earthquake and the shipment of humanitarian aid (Fig 3e). In addition, asphalt and reinforced concrete roads had transverse fractures to the axis of the lateral access road to the city of Jama. There, the macroseismic intensity assigned was IX, when applying the environmental intensity scale ESI-2007 (Michetti et al., 2007; Chunga et al., 2018).

5. Geological and Geophysical characterization of the subsoil

A geological profile (A-B) with a length of 2.8 km, trending NW-SE has been performed for the urban area of the city of Jama, where most of the damage to buildings occurred during the M 7.8 Pedernales earthquake in 2016 (Fig. 4). The profile is located on alluvial plain deposits in the sedimentary deposition domain of an alluvial valley limited by hillside zones.

The first layer of artificial fill and waste materials is between 1 and 2 meters height, being attributed to a modern anthropogenic soil. Several Quaternary geological units have been recognized in the area, such as the alluvium plain deposits (Qa) that have a thickness ranging between 2 to 4 m, conformed by MH and CL soils of Holocene age. The shear velocity from microtremor ranges from 110 to 150 m/ s. The colluvium deposits (Qc) are constituted by ML soils, being of Late Pleistocene age, with thicknesses between 8 to 15 m, and a shear velocity from 200 to 260 m/s. This unit can be divided into two subunits, being more recent colluvial where the N60 reach values of 30, and older and more resistant sediments where the N60 reach values of 50.

The ancient alluvium plain deposits (Qaa) are constituted by firm soft soils ML, MH and SM, with Holocene to Late Pleistocene ages, and thickness between 6 to 8 m their shear velocity ranges from 160 to 210 m/s. In this unit, the rigid silt layer reaches N60 values reaching 60 strokes, being the most resistant layer in the entire Middle - Upper Pleistocene sequence.

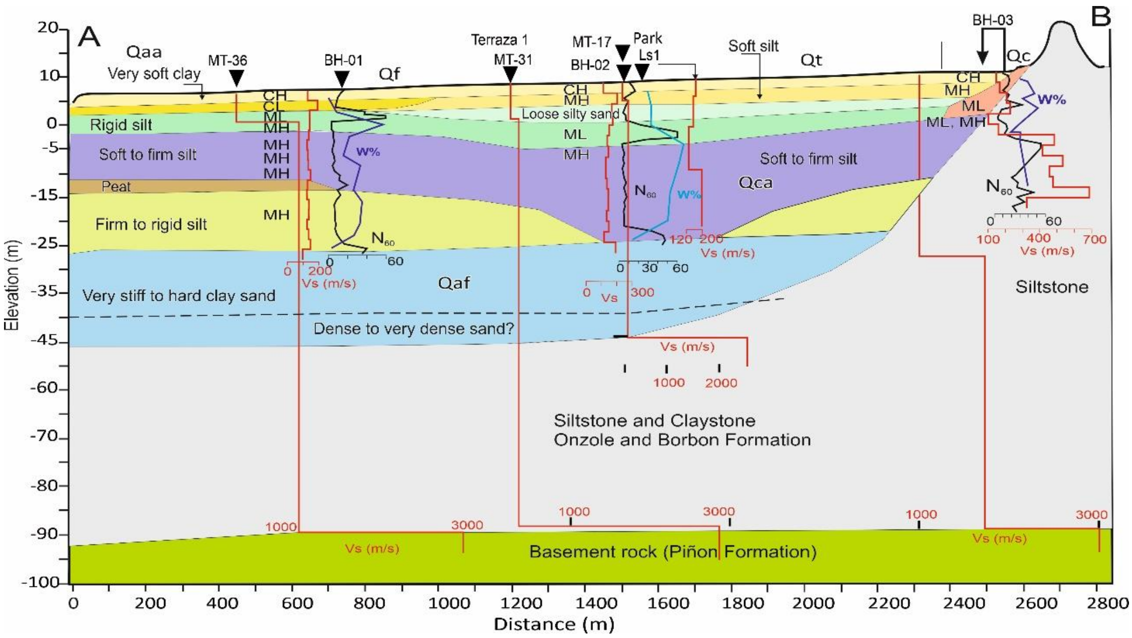

Figure 4. Geological - geoseismic section A-B of the urban area of Jama.

The loose silty sand layer, being 3 m thick, may indicate a phase of marine transgression. The colluvium alluvium deposits (Qca) of Late Pleistocene age, is between 10 to 25 m thick, with a soil type of MH and OH, while the shear velocity ranges between 130 to 200 m/s. At the base of this unit, a layer of firm to rigid silt may be associated with a progradational deposition being later eroded by the colluvial alluvial deposits. Here is where the number of blows reached values of 10 N60 and shear velocity in the range of 100 to 120 m/s. A layer of peat is differentiated in this geological unit. Finally, the alluvial valley-fill deposits (Qaf) have older soils of Middle Pleistocene age, being originated of probably marine fluvial deposition, of SM and SC type, from moderate dense to dense sand and rigid to hard clay sand, with a thickness between 15 and 40 m and Vs values between 260 and 450 m / s. The number of strokes reached values of 40 N60.

Table 3. Stratigraphic column of the Jama Canton

Geologic units	Thickness of sediments	Uscs soil type	Geological age	Average shear velocity
Fill	1≤m≤2	CH / waste materials	Modern	100≤Vs≤140
Intertidal flat, alluvium plain and ancient floodplain deposits (Qa - Qaa - Qf)	2≤m≤4	MH, CL	Holocene	110≤Vs≤150
Terrace (abandoned floodplain deposits) (Qt)	6≤m≤8	ML, SM	Holocene to Late Pleistocene	160≤Vs≤210
Colluvium deposits (Qc)	8≤m≤15	ML	Holocene to Late Pleistocene	200≤Vs≤260
Ancient colluvium alluvium deposits (Qca)	10≤m≤25	MH, OH	Late Pleistocene	130≤Vs≤260
Alluvial valley fill deposits (Qaf)	15≤m≤40	SC, SM	Middle Pleistocene	260≤Vs≤450
Soft rock (Mab)	40≤m≤100	siltstone, claystone	Miocene	380≤Vs≤680
Basement rock (Kp)	> 40m	basalt	Cretaceous	1000≤Vs≤3000

The rocky basement of Miocene age is constituted by siltstones and claystones of the Onzole and Borbon geological formation (Stainforth, 1948; Whittaker, 1988), where the shear velocity must be around 680 m/s. Results obtained from active seismic methods indicate that the Miocene rocks are between 40 and 100 m thick, delineating the lithological contact of the cretaceous basaltic basement between 90 and 100 m deep from the surface (Chunga, 2019; Daza et al., 2019), and where the *Vs* reach 2,800 m/s. Table 3, lists the characteristics of the geological materials of the six Quaternary units of Jama city and the Onzole, Bobon and Piñon geological formations.

6. Geotechnical soil characterization and liquefaction susceptibility

The consequences of liquefaction may be very different according to site characteristics and being classified. Furthermore, liquefaction may occur due to cyclical mobility and flow (Kramer, 1996). Cyclic mobility is the phenomenon in which there is a progressive increase in pore pressure until it equals the effective confining pressure, this means, there is an accumulation of deformation but it does not fail and what exists is a loss of rigidity. Such phenomenon is able to cause considerable damage to the structure (Osorio, 2009).

The flow failure is generated by a sudden loss of resistance to an increase in pore pressure caused by the undrained stress. In addition, there are excessive deformation. Therefore, when considering flow failure, it refers to a loss of resistance in which the mass of soils is required to be subjected to a static shear stress greater than the undrained shear strength. Compared with that of cyclical mobility, the effects of flow failure can be classified as catastrophic (Kramer, 1996).

In order to occur flow liquefaction, the geotechnical criteria of having the soil saturated 100% need to be met. This is mostly the case, if there is an undrained load which originates from different sources such as a seismic load from an earthquake of moderate to strong magnitude, or through waves that may be caused by construction systems such as an explosion or vibrations that are used for geotechnical improvement of soils or in the driving of piles that are also sources of waves. Other conditions are that the tendency of the soil during cutting is contractive and that the soil is susceptible to liquefy. These soils may be clean and uniform sands, usually non-plastic silts and, in rare cases, gravels and clays that are also able to liquefy but with little to none catastrophic effects (Osorio, 2009).

In the current study, the liquefaction susceptibility is being analyzed for soils that reported previously coseismic damage during the 2016 earthquake. The epicenter of the M 7.8 earthquake was located some 50 km NE of the city of Jama. Several researchers of earthquake engineering have studied the liquefaction susceptibility of geologic units of recent environmental depositions, proposing criteria for their classification (Youd and Perkins, 1978; Wakamatsu, 1992; CDMG 1999).

According to these guidelines, the Jama urban area is meeting the following criteria: (a) the urban area appears to have been constructed on the geological units such as alluvium plain and abandoned floodplain deposits, of Holocene to late Pleistocene age; (b) the groundwater is less than 5 meters deep and the peak ground acceleration (PGA) has a 10% probability of being exceeded in 50 years in the range between 0.45 and 0.55g (NEC-11, 2015; Garcia et al., 2016; Parra et al., 2016; Beauval et al., 2018); (c) evidence of historical liquefaction surely were reported after the May 13, 1942 (M 7.9) and the April 16, 2016 (M 7.8) megathrust earthquakes (Swenson and Beck, 1996; Ye et al., 2016; Toulkeridis et al., 2017; Chunga et al., 2018). In liquefaction studies it is important to determine the depth of the potentially liquefiable strata, and of these, which layer may have greater probability of liquefaction (Salocchi et al., 2020). In the current study, the maximum probability will be determined of liquefaction in deep strata.

As a first approach, particular attention is referred to the stratigraphy of the urban area, using a variety of study techniques (Seed et al., 2003; Chen and Juang, 2000; Juang et al., 2003). Then, the empirical approach of these stratigraphic units are classified as "probably liquefiable", when the liquid limit is less than 37% and its plasticity index is less than 12% (Seed, 2003), always that the water content is high (wc > 0.8 LL). Consequently, a re-evaluation of the geotechnical parameters from three boreholes was conducted (BH1, BH2 and BH3). The Municipality of Jama, and the University of Los Andes from Colombia and some private soil laboratories provided the geotechnical information required for estimating the liquefaction potential according to the proposed methodologies (Wang, 1979; Seed and Idriss, 1982; Chen and Juang, 2000; Juang et al., 2000) have provided these data (Chunga, 2019; Daza et al., 2019).

Hereby, the majority of the perforations (boreholes) are delineated in the liquefiable area (Seed et al., 2003). However, this criterion is not fully compatible with the low plasticity behavior of fine-sized soils of the Jama city, where historical evidence of liquefaction has been documented in the alluvium plain and abandoned floodplain deposits. Figure 5, illustrates the results of the Liquidity index and the water content of the soil of the city of Jama, allowing to determine the scale of the natural moisture content of the soil samples with reference to the liquid and plastic limits. Hereby, it provides an indicator of geological history presenting these soils with ultra-sensitive sand deposits.

The analysis for the urban area of the city of Jama demonstrates that there is a deep stratum of late Pleistocene age which may also be potentially liquefiable when the soils meet a saturation close to 100%. The statistical summary of all these geotechnical parameters for the city of Jama is given in table 4. From the results listed in this table and the particle size distribution results (Fig. 5), the following statements may be made: (a) the saturation in alluvium plain deposits is about 95% whilst for the ancient alluvium deposits it is about 85%; (b) the fraction of fines particles (Fc) ranges between 1% to 61% for alluvium plain deposits and from 75% to 97% for the ancient alluvium deposits; (c) the diameters with 50%, D50, is between 0.02-0.20 mm for alluvium plain and ancient alluvium; (d) the coefficient of uniformity (CU) lies between 1.7 and 2.1 and the degree of curvature between 0.8 and 2.5 for fine to coarse silt and fine sand according to the soil classification.

The analysis of the previous data indicates that the alluvium plain and abandoned floodplain (terrace) deposits are the liquefiable soils of the area (Fig. 4). The distribution of the SPT values in function of depth in the urban area of the city of Jama is illustrated in Figure 5.

7. Results and discussion

7.1. Evaluation of the liquefaction potential

To evaluate the earthquake-induced liquefaction potential of the Late Pleistocene - Holocene geological units in the city of Jama, some risk-based methods from an SPT-based simplified procedure and shear wave velocity seismic measurements were considered. These methods were originally developed by Seed and Idriss (1971) and updated and modified later (Seed et al., 1985; Youd and Idriss, 1997; Youd et al., 2001). These deterministic methods comprise the calculation of the safety factor per layer (FS), defined as the ratio between cyclic resistance ratio (CRR) and the cyclic stress ratio (CSR).

$$FS = {}^{CRR}/_{CSR} \tag{7}$$

The CRR, according to Youd and Idriss (2001) is calculated using the following equation:

$$CRR = \frac{1}{34-(\text{N1})\ 60} + \frac{(N1)60}{135} + \frac{50}{(10\text{x}(N1)60+45)^2} - \frac{1}{200} \qquad (8)$$

Where, (N1)60 is influenced by the measured standard penetration resistance N, relative to the overburden pressure factor (Cn), the correction for hammer energy ratio (ER) Ce, the correction for borehole diameter Cb, the correction factor for rod length Cr, and the correction for samplers with or without liners Cs. The Cn was calculated according to the equation proposed by Liao and Whitman (1986), Cn = (Pa/σ′v)0.5 in function with (Pa) (atmospheric pressure) and the σ′v (effective vertical stress). Afterward, a "fine content" correction was applied to the calculated N1(60) value in order to obtain a clean-sand-equivalent value N1(60) Cs given by the equations proposed by Youd et al. (2001) as illustrated in figure 5.

The CSR defines the seismic demand and is expressed as:

$$CSR = \frac{0.65\left(\frac{amax}{(g)}\right).(\frac{\sigma v}{\sigma' v})(rd)}{MSF} \qquad (9)$$

Where σv is the total vertical stress at depth z, σ′v is the effective vertical stress at the same depth, amax is the peak horizontal ground acceleration, (g) is the acceleration due to gravity, and rd is the stress reduction factor. In this study, the term "rd" was estimated using the Liao and Whitman (1986) equation:

rd= 1.0 - 0.00765xZ for Z ≤ 9.15 m (10)

rd= 1.174 - 0.0267xZ for 9 .15 m ≤ Z ≤ 23m (11)

Then, the CSR values have been divided by the magnitude scaling factor (MSF), which is calculated by the following equation, Youd et al. (2001):

MSF = (M/7.5)2.56 (12)

Furthermore, Chen and Juang (2000) developed a simplified equation for CRR based on their neural network analysis of field observations:

CRR7.5 = 0.241 {exp[(0.032+0.004FCI) (N1)60]} -0.182 (13)

Where FCI is an index of fines content (FC) defined as follows: FCI = 1 for FC<5%, FCI =2 for 5%<FC<12%, FCI =3 for 12%<FC<35%, and FCI = 4 for FC>35%. The use of the ordinal scale to characterize the effect of fines content is consistent with current geotechnical knowledge (Chen and Juang, 2000). Thevalues of, CSR and CRR will bring us to the estimation of safety factor (FS). The results of the safety factor (FS), for the different geological units in the city of Jama are illustrated in Table 4. All the soil layers with a safety factor higher than 1.25 are considered as non-liquefiable soil layer according to Seed and Idriss (1982). Below the suggested value (1.25) the soil layer is considered to be prone to experiment liquefaction, Complying the liquefaction susceptibility criteria suggested by Chen and Juang (2000) and Juang et al. (2003).

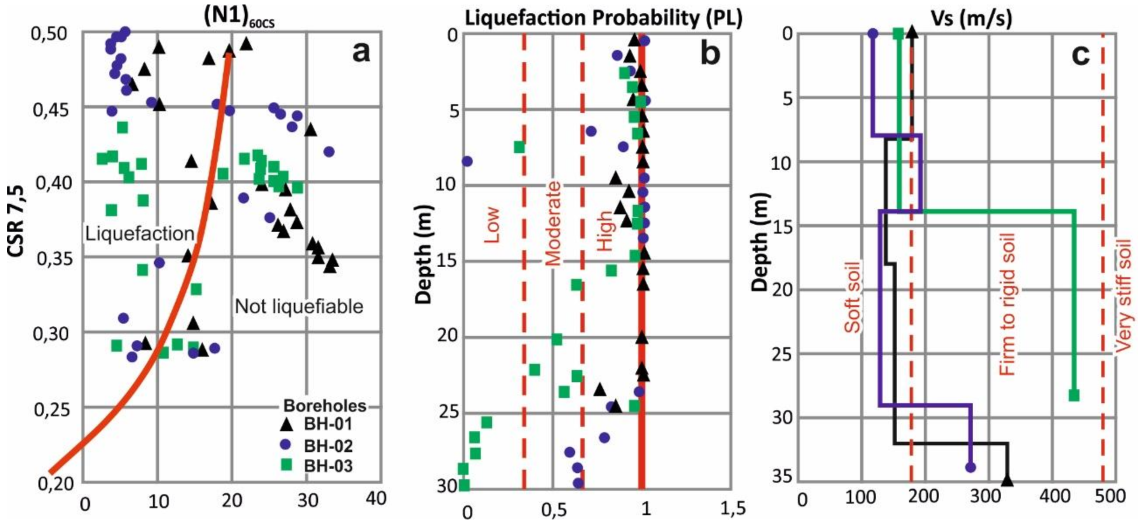

Figure 5. **a)** Relationship between the Cyclic Stress Ratio (CSR) causing liquefaction and the value (N1) 60cs for silty sands. **b)** Calculations obtained of liquefaction probability PL for sands from geoengineering drilling for the city of Jama. **c)** Evaluation of S-velocity (Vs) to a depth of 35 m.

7.2. Liquefaction potential mapping

Although the available stratigraphic information reaches 35 m of depth, the recorded coseismic deformations in the soils of Jama are less than 20 m deep. Therefore, a depth of 20 m has been considered for the liquefaction potential assessment. The Liquefaction potential index (LPI) has been calculated in the urban area of Jama using the equation defined by Iwasaki (1982) as:

$$LPI = \int_0^Z F(z)W(z)_{dz} \qquad (14)$$

Where z is the depth below the ground surface in meters and is calculated as w(z)=10-0.5z; F(z) is a function of the safety factor and the liquefaction factor, FS, where F(z) =1-FS when FS<1 and if FS>1 than F(z)=0. Iwasaki et al. (1982), calibrated the severity of liquefaction induced damages as follows, LPI=0 as not prone to liquefaction 0<LPI<2, 2<LPI<5, 5<LPI<15 and LPI >15 as low, moderate, high, and very high susceptibility to liquefaction, respectively.

The probability of liquefaction was calculated for all the boreholes using the logistic regression proposed by Chen and Juang (2000) and modified by Juang et al. (2003):

$$\text{Probability (liquefaction)} = \frac{1}{1+\left(\frac{Fs}{0.96}\right)4.5} \qquad (15)$$

The results of the liquefaction probability for the different boreholes are listed in Table 4 and Figure 5. These findings were interpreted showing that in the urban area of Jama city there is a high probability that "almost certain" soil liquefaction will occur in the Holocene sedimentary layers according to the method proposed by Iwasaki et al. (1982). Also, there are very likely sectors where no soil liquefaction will occur.

The liquefaction susceptibility of the urban area of the city of Jama was calculated considering the data of the previous section. This result delineates the areas according to their probability of liquefaction. The liquefaction probability mapping of the area of study is obtained by interpolation of the liquefaction potential index (LPI) obtained for each borehole, and processed with the Arc-Map GIS and Surfer software. The coseismic liquefaction evidences of the Pedernales earthquake (M 7.8) are confronted with the results of the LPI data (Iwasaki et al., 1982).

Regarding the geological section, the recent alluvium plain and ancient floodplain deposits have (referring to the location of BH-01) a very high probability of liquefaction up to 15 m depth (0.85≤PL≤1.00; 0.653≥FS> 0.000). In the interface zone with the ancient alluvial plain deposits, the probability of liquefaction is moderate with up to 23 m depth (0.35≤PL≤0.65; 1.102≥FS> 0.837), while beyond that depth, the ancient colluvium alluvium deposits, the probability of liquefaction is zero (0.00≤PL≤0.15; ∞≥FS> 1.411).

In the central park of Jama (referred to the location of drilling BH-02), the lithological units of ancient floodplain and abandoned floodplain (terrace) deposits have greater thicknesses, as paleo-channels are evidenced in seismic refraction profiles. Recent alluvium plain deposits have a very high probability of liquefaction up to 6 m depth, leveed channels of silty sand of 1m height have a high probability of liquefaction (0.65≤PL≤0.85; 0.837≥FS>0.653). The sedimentary depositions of greater thickness in paleo-channels are filled by ancient fllodplain deposits. In this unit the probability of liquefaction is moderated down to 25 m of depth, while beyond that depth, the sediments are classified asvery rigid to hard clay sands, having zero probability of liquefaction.

The colluvial soils have thicknesses between 8 and 15 m, while underlying this lithological unit ancient alluvial plain deposits are found (referring to its location to well BH-03). In these two units the probability of liquefaction is high to very high, moving deeper to 23 m depth. Beyond that depth until 30 m, ancient colluvium alluvium deposits, from firm to rigid silt, have a low probability of liquefaction (0.15≤PL≤0.35; 1.411≥FS> 1.102). The probability of liquefaction of soil strata and safety factors have been interpreted based on the classification proposed by Chen and Juang (2000).

These results reveal that the urban area of Jama presents soils with high liquefaction potential. The liquefaction probability (PL) are delineated for those recent sedimentary depositions like alluvium plain, ancient floodplain and abandoned floodplain deposits of late Pleistocene - Holocene age, where the geological and hydrological conditions are favorable for ground-coseismic liquefaction (Table 4 and Figure 5).

Table 4. The classification of the probability of liquefaction as proposed by chen and juang (2000).

Probability (PL)	**Description**	**Safety Factor**	**Liquefaction Hazard Level**
0.85 ≤ PL< 1.00	Almost certain that it will liquefy	0.653 ≥ FS > 0.000	Very high
0.65 ≤ PL< 0.85	Very likely	0.837 ≥ FS > 0.653	High
0.35 ≤ PL< 0.65	Liquefaction / non liquefaction is equally likely	1.102 ≥ FS > 0.837	Moderate
0.15 ≤ PL< 0.35	Unlikely	1.411 ≥ FS > 1.102	Low
0.00 ≤ PL< 0.15	Almost certain that it will not liquefy	α≥ FS > 1.41	Very low to null

7.3. Site response analysis

The city of Jama is located in zone VI signifying a high seismic level with a factor of 0.5g, with a 10% exceedance in 50 years and a return period of 475 years (NEC-11, 2015). The V_{S30} seismic data were obtained from downhole geophysical tests, indicating a better contrast in the stratigraphy of the alluvial and alluvial-colluvial soils of Jama. For colluvial soils, up to a depth of 15 meters, shear wave velocities higher than 300 m/s were measured, while moving further below to older colluvium alluvium and alluvial valley deposits of medium consistency, where the velocities reached 440 m/s. Shear wave velocity is the most important variable when establishing how the ground will behave in the event of seismic excitation. Therefore, it is vital to have extensive information and knowledge of the shear wave velocity profiles for the different perforations.

With these geotechnical characteristics and corroborating the technical specifications of the NEC-11 (2015), the soils of Jama are classified as geotechnical Type D. For recent alluvial and floodplain soils, there are granular levels between 10 and 15 meters of depth, then up to 28m their velocity are reduced to 120 m/s. In this interval, sediments of medium consistency begin with shear wave velocity up to 320 m/s. The geotechnical classification for these soil is type E (NEC-11, 2015).

Furthermore, the seismic zone factor Z has been obtained for more resistant soils (greater than 30 m in depth), designating the C profile for the geological units of ancient colluvium alluvium and alluvial valley fill deposits. These units meet the velocity criteria according to NEC-11 (2015), with values that fluctuate between $760 \geq Vs \geq 360\ m/s$, and the considerations of the soil amplification coefficients Fa, Fd , Fs, reflecting a layer with characteristics of dense to very dense non cohesive soil. With these, an elastic response spectrum of accelerations Sa is determined, expressed as a fraction of gravity and the different types of sedimentary units in the city of Jama (Fig. 6, 7, 8, 9, 10; Supplementary Materials).

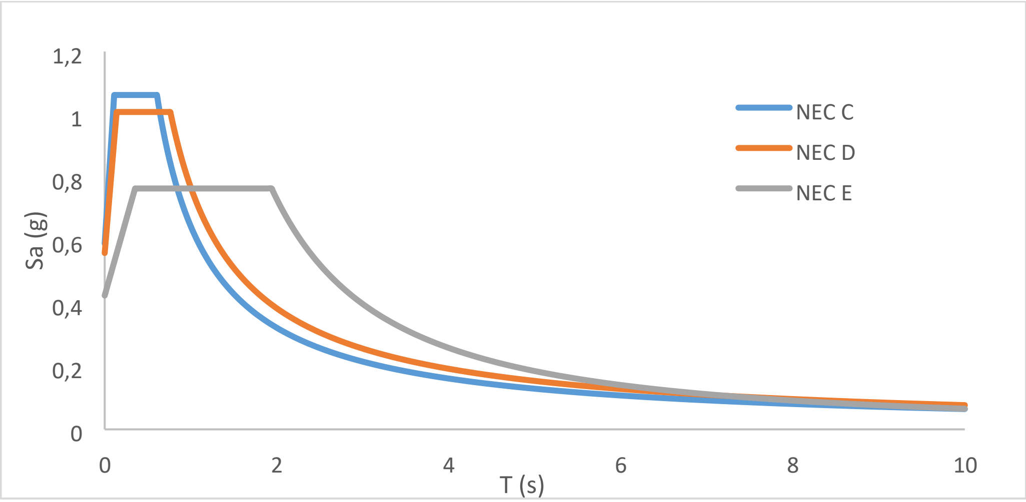

Figure 6. Elastic seismic spectra of NEC (2015) accelerations for soil and rock profiles.

The active seismic data allowed the estimation of the soil/rock contact for Quaternary deposits, between 50 to 55 meters depth, and for colluvial soils, between 8 and 15 meters depth. The predominant rocks in the area are claystones from the Onzole formation of Tertiary age, below the volcanic basement of Cretaceous basalts of the Piñon formation (Baldock, 1985; Proust et al., 2016).

7.4. Selection of earthquakes with compressive tectonic settings

For this earthquake analysis, ten earthquakes with similar tectonic characteristics have been selected for the Jama canton, central region of Manabí. Therefore, the PEER ground motion database was used, in which the period coordinates and spectral accelerations were entered as target spectrum, of the NEC-11 (2015) spectrum (Supplementary Materials), for soil types C (dense soil or soft rock). The Chi Chi earthquake in Taiwan of M 7.6, associated with a seismogenic structure with inverse tectonic stresses, and a rupture surface of 80 km (Lee et al., 2002), has been selected for our site response analysis, considering ten seismic records with different horizontal components. The seismic traces for the vertical components have not been considered in this study, due to its low probability of significant earthquake environmental effects. Subsequently, a calibration of the scale factors was performed for the selected earthquakes, maintaining at all times a scale factor of 1 to 3, for a return period (Tr) of 475 years, as presented in Figure 7, and shows the seismological characteristics of the scaled movements.

The seismogenic structures allow the estimation of the maximum magnitudes and accelerations expected in rocks (Romeo and Pugliese, 2000; Douglas, 2003; Ambraseys et al., 2005). Hence, the movement prediction in the ground under the action of a seismic event is typically obtained by an one-dimensional site response analysis. These analysis are usually performed using equivalent linear models since it requires direct properties of the soils and a simple computational calculation. One of the most well-known and calibrated linear equivalent models is implemented in the Deepsoil software (Hashash, 2016), which calculates the response of a system of homogeneous, viscoelastic layers of an infinite horizontal limit, subjected to a motion of the shear wave traveling vertically.

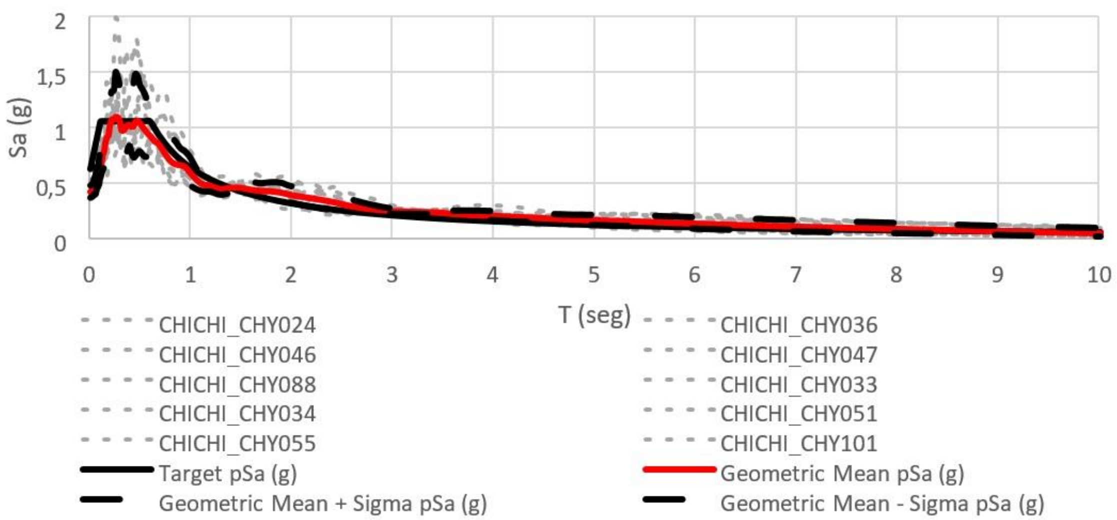

Figure 7. Elastic seismic spectra Acceleration response spectrum (5% structural damping) for ten scaled seismic movements (gray lines) for inverse component earthquakes, with seismological characteristics similar to the expected uniform hazard spectrum, 10% probability of exceedance in 50 years, the median and median ± 1 standard deviation of the scaled movements for NEC-type rock profile.

The non-linearity of the soil is represented by the use of the equivalent linear soil properties through an iterative process. In the Linear Equivalent model process a rock outcrop motion, typically a recorded motion at the surface, is taken and converted into an "internal rock motion". This "internal" rock movement is then converted from the time domain that is, a temporal evolution of accelerations, to the frequency domain, while adding harmonic waves of different frequencies where each has its own amplitude. However, under a compatible base rock condition, where the impedance ratio is not infinite, an "internal" rock movement can be affected by the impedance ratio of the rock-soil interface, the mass of the soil deposit and its response characteristics, such as the characteristic period (Schnabel et al., 1972).

The appropriate shear modulus and damping value, which are dependent on deformations, are set for each layer during each iteration. When convergence is reached, the problem turns to a viscoelastic material with constant properties. With these constant shear modulus, damping, and unit weight values for each layer, the wave equation can be solved using a complex stiffness response method. A transfer function based on this model is calculated to relate the movement at the base level, that is, internal rock movement, to the movement at the ground surface.

Regarding the stress-strain cyclical hysterical behavior of the models, these can be validated with laboratory curves available in the literature, in this specific case Vucetic & Dobry, 1991, were used for the fine fraction and Seed & Idris, 1991 for the coarse fraction, which provides the degradation curves of the shear modulus G / Gmax (-) and the% damping ratio are obtained with the deepsoil V7 program.

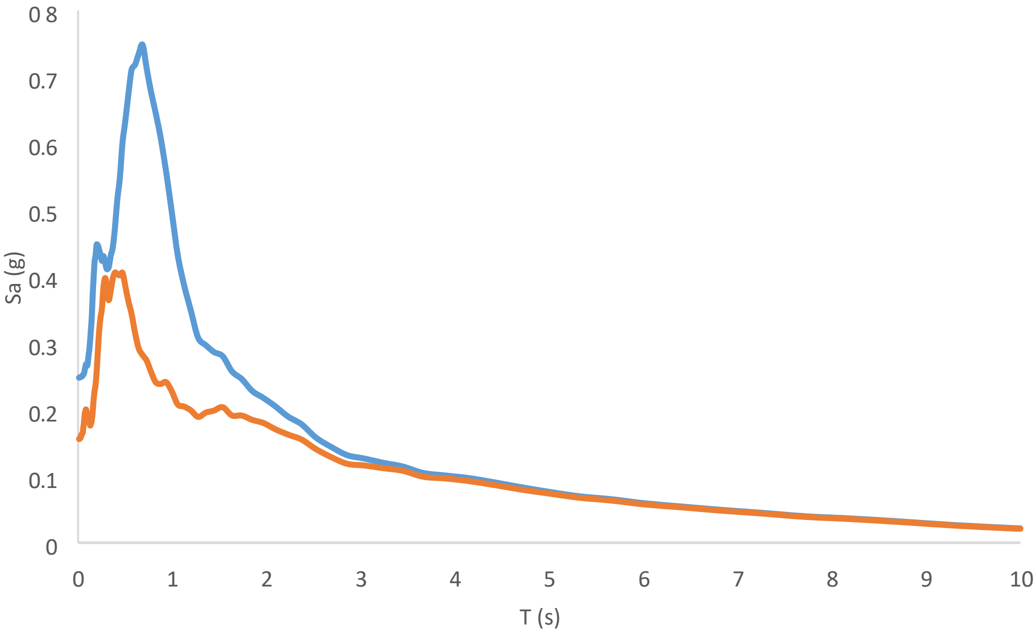

Figure 8. Rock and coluvial strata surface response spectrum for the BH-03 well. Colors represent: the blue color the surface data and the orange line the rock data.

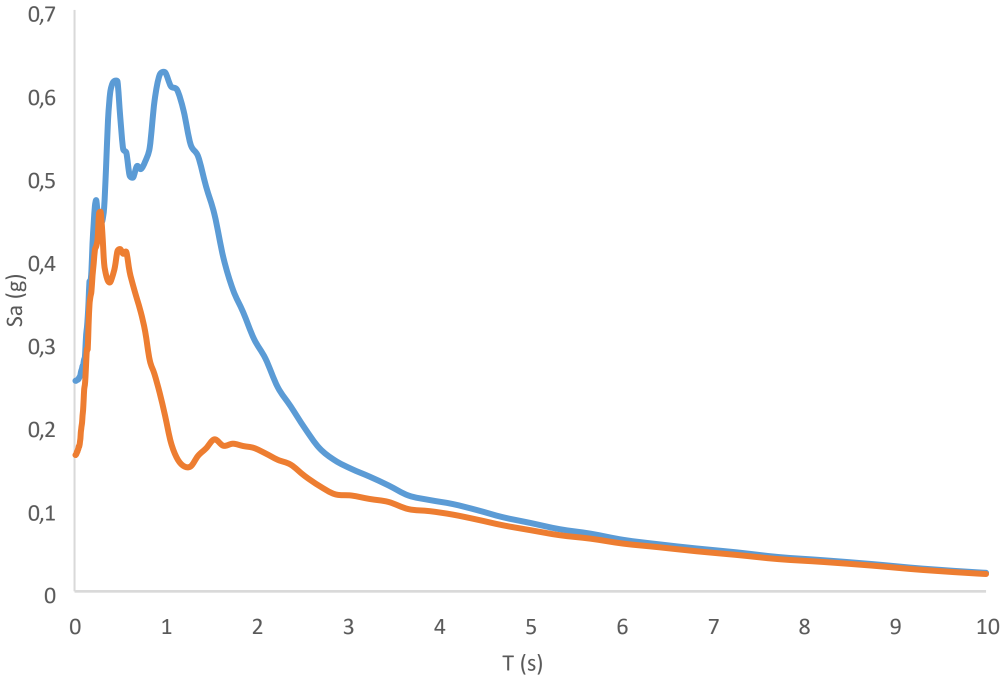

Figure 9. Rock and floodplain strata surface response spectrum for the BH-01 borehole. Colors represent: the blue color the surface data and the orange line the rock data.

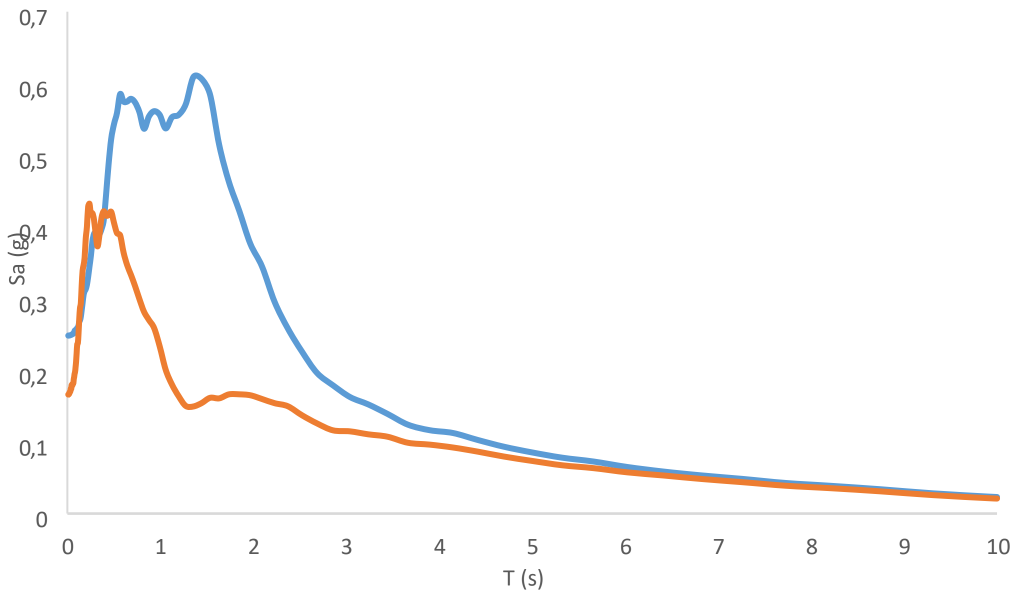

Figure 10. Rock and abandoned floodplain strata Surface Response Spectrum for BH-02 sounding. Colors represent: the blue color the surface data and the orange line the rock data.

The geometric mean of the spectra of elastic acceleration responses obtained for the horizontal components of the earthquakes compatible for the Profile D and E soils are presented. With return periods of 475 years for the Equivalent linear analysis for these spectra has been considered a structural damping equal to 5%. The inclusion of the geometric mean of the selected records allowed us to appreciate the amplification that occurs due to the diverse depositional environmental strata found at the site. For the units of colluvial sediments (referred to BH-03), the spectral accelerations of 1.68g was obtained for a period between 0.5s and 0.7 s, while for the recent alluvial and floodplain sediments (referred to BH-01), a peak acceleration of 1.04g was obtained for periods between 0.87s and 1.11s.

Finally, for the ancient alluvial and abandoned flooplain sediments (referred to BH-02, central park of Jama) confirms an acceleration of 1.03g was obtained for periods between 1.3 and 1.5s. In this context, the thickness of Quaternary deposits has a direct impact on the fundamental vibration period of the deposit and; therefore on the shape and the expected spectral amplification, being a variable that generates high sensitivity.

Therefore, we may conclude that in the analysis indicated in the spectra obtained on the surface are greater than those of the acceleration plateau of the Ecuadorian Construction Regulations (NEC-11, 2015). Additional graphs have been obtained where the response spectra at the top of the rock are compared as well as with the spectra of the soil profiles. Graphs were generated demonstrating the response comparison both on the surface and on the rock for the three boreholes.

8. Conclusions

The city of Jama is located in a high sesmicity area, having rock accelerations, GPA-rock of 0.5 g ang over and, its ground amplification can be in the range of 1.05 and 1.68 g. In this study, historical data from previous earthquakes was appraised, revealing a short frecuency for earthquakes with magnitudes over 7.6, showing that the constructions located in the urban area could be affected in this scenario. The data collected from the Jama earthquake in 1942 with M 7.9, and Pedernales 2016 with M 7.8, registered coseismic geologic effects such as soil liquefaction, that were the porpose of this study.

The liquefaction potential of the soil in the urban area of the city of Jama, was estimated using on site data collected after the 2016 earthquake. Three main data bases were used, 1) The seismotectyonic, 2) The geologic background in Jama and 3) The Stratigrafic information obtained from three ground perforations.

After performing the liquefaction potential assessment method, the data obtained was processed in GIS, to generate the liquefaction hazard map by plotting the liquefaction potential index, LPI. These quantitative results demonstrated that the main urban area exhibits a high liquefaction potential. The city appears to be constructed over a recent alluvial plain and an abandoned foodplain. Recent colluvial deposits have a very high probability of liquefaction down to 15 m depth, considering a maximum acceleration of 0.5 g for the urban area of Jama.

The results highlighted the importance of geotechnical assessments of particular geological environments which have sediments prone to liquefaction. This tool provides a better understanding of how the constructions and buildings could be affected by an earthquake of high magnitude depending on the type of soil. This was a non existing tool that could help engineers to improve urban area planification or buildings stabilization to lessen the severity on earthquake's effects in the city of Jama and other areas with similar geological conditions. It is important to mention that, the areas displayed in the liquefaction hazard map were contrasted with the on site data collected after the Pedernales earthquake.

For the dynamic response modeling of the soil profile, it was necessary to have different parameters that described the geotechnical characteristics of the profile. However, it was evidenced that the shear wave velocity is the variable with the greatest weight when establishing how the soil is going to behave due to seismic excitation. Thus, for colluvial soils there are higher spectral amplifications of 1.68g with periods between 0.5 and 0.7 seconds. The obtained results indicate that soil deposits tend to have important degradations at high acceleration levels. Therefore, if the intensity level of the input signal increases, the maximum spectral amplification peaks will be at higher structural periods and will have amplitudes lower due to the increased hysteretic damping of the soil. Since, by presenting low wave velocity and clay soils with high plasticity in the soil profiles, a very high loss of shear stiffness will be common due to the deformations imposed by the input signals.

The elastic design spectra was analyzed for a return period of 475 years, considering a level of structural damping equal to 5% and corresponding to an on site response, that is, the interaction between soil and soil has not been considered foundation of the structure. For the structural calculation, it would be recommended to use an envelope of the spectra obtained in each of the analysis. Site response analysis was performed using the Linear Equivalent method and in terms of Effective Vertical Stress.

9. Data and resources:

Seismicity and macroseismic data were collected from IGEPN (http://www.igepn.edu.ec/servicios/eq20160416, last accessed June 2020),

USGS (http://earthquake.usgs.gov/earthquakes/eventpage/us20005j32#dyfi, last accessed May 2019) and the Geological Survey of Colombia (http://studylib.es/doc/6527439/informe-del-sismo-del-16-de-abril-de-2016-en, last accessed June 2020).

PEER Ground Motion Database (Earthquake records from PEER NGA strong motion database, https://ngawest2.berkeley.edu/, last accessed Sept 2020).

The DTM used for analysis is the NASA SRTM 3.0 global model, 1 arc second resolution: https://lpdaac.usgs.gov/news/nasa-shuttle-radar-topography-mission-srtm-version-30-srtm-plus-product-release/ (last accessed 22 August, 2020).

Some of the figures were realized using Qgis and Arcmap® software.

Supplementary Materials: Liquefaction analysis and site response

Author Contributions: D.A. and E.O.H. designed the study. E.V. and T.T. analysed the geomorphologic features and liquefaction probability, D.A. and D.D.T. processed and analysed the site seismic response. K.C. and G.M.D. prepared the manuscript with advice and feedback from all team members.

Funding: This research received no external funding.

Acknowledgements: This work was supported by the Geohazard Research Group of the Universidad Técnica de Manabí (UTM).

Conflicts of interest: The authors wish to confirm that there are no known conflicts of interests associated with this publication. This research did not receive any specific grant from funding agencies in the public, commercial, or not-for-profit sectors.

10. References

[1] Swenson, J. L., and S. L. Beck (1996). Historical 1942 Ecuador and 1942 Peru subduction earthquakes and earthquake cycles along Colombia-Ecuador and Peru subduction segments. Pure Appl. Geophys. 146(1) 67-101.

[2] Obermeier, S.F. (1996). Use of Liquefaction-Induced Features for Paleo Seismic Analysis—An Overview of How Seismic Liquefaction Features Can Be Distinguished from Other Features and How Their Origin Can Be Used to Infer the Location and Strength of Holocene Paleo-Earthquakes. Engineering Geology, 44, 1-76. http://dx.doi.org/10.1016/S0013-7952(96)00040-3.

[3] Egred, J. (2009). Catálogo de Terremotos del Ecuador 1541–2009, Internal Report, Escuela Politecnica Nacional, Instituto Geofisico.

[4] Toulkeridis, T., 2016: Unexpected results of a seismic hazard evaluation applied to a modern hydroelectric plant in central Ecuador. Journal of Structural Engineering, 43, (4): 373-380.

[5] Aguiar R, Mieles Bravo Y (2016) Análisis de los edificios que colapsaron en Portoviejo durante el terremoto del 16 de abril de 2016. Revista Internacional de Ingeniería de Estructuras 21(3):257–282

[6] Chunga, K., T. Toulkeridis, X. Vera-Grunauer, M. Gutierrez, N. Cahuana, and A. Alvarez (2017). A review of earthquakes and tsunami records and characterization of capable faults on the northwestern coast of Ecuador, J. Sci. Tsunami Hazards 36, no. 3, 100–127.

[7] Moncayo Theurer, M., Velasco, G., Mora, Carlos, Montenegro, M., Cordova, J. (2017). Terremotos mayores a 6.5 en escala Richter ocurridos en Ecuador desde 1900 hasta 1970. Ingeniería, 21. http://www.redalyc.org/articulo.oa?id=46753192005> ISSN 1665-529X.

[8] Navas, L., Caiza, P. and Toulkeridis, T., 2018: An evaluated comparison between the molecule and steel framing construction systems – Implications for the seismic vulnerable Ecuador. Malaysian Construct. Res. J. 26 (3), 87–109.

[9] Cando-Jácome, M., Martínez-Graña, A. (2019). Differential interferometry, structural lineaments and terrain deformation analysis applied in Zero Zone 2016 Earthquake (Manta, Ecuador). Environ Earth Sci 78, 499, doi:10.1007/s12665-019-8517-4.

[10] Serva, L. (2019). History of the Environmental Seismic Intensity Scale ESI-07. Geosciences 9(5): 210, doi:10.3390/geosciences9050210.

[11] Vera-Grunauer X., Lopez-Zhindon S., Ordoñez-Rendon J., Chavez-Abril M.A. (2019). Liquefaction case histories after the 2016 megathrust Pedernales earthquake in Ecuador. Earthquake Geotechnical Engineering for Protection and Development of Environment and Constructions – Silvestri & Moraci (Eds). Associazione Geotecnica Italiana, Rome, Italy, ISBN 978-0-367-14328-2

[12] Giesecke, A., A. G. Capera, I. Leschiutta, E. Migliorini, and L. R. Valverde (2004). The CERESIS earthquake catalogue and database of the Andean Region: background, characteristics and examples of use. Ann. Geophys. 47(2-3).

[13] Michetti, A. M., E. Esposito, L. Guerrieri, S. Porfido, L. Serva, R. Tatevossian, E. Vittori, F. Audemard, T. Azuma, J. Clague, et al. (2007). Environmental Seismic Intensity Scale 2007—ESI 2007, Memorie Descrittive della Carta Geologica d'Italia, Vol. 74, Servizio Geologico d'Italia– Dipartimento Difesa del Suolo, APAT, Rome, Italy,7–54, available at http://www.isprambiente.gov.it/en/publications/technical-periodicals/descriptive-memories-of-the-geological-map-of/intensity-scale-esi-2007?set_language=en (last accessed August 2018).

[14] Berzhinskii, Y. A., A. P. Ordynskaya, A. S. Gladkov, O. V. Lunina, L. P. Berzhinskaya, N. A. Radziminovich, Y. B. Radziminovich, V. S. Imayev, A. V. Chipizubov, and O. P. Smekalin (2010). Application of the ESI-2007 scale for estimating the intensity of the Kultuk earthquake, August 27, 2008 (south Baikal), Seismic Instrum. 46 307–324.

[15] Kelson, K., R. C. Witter, A. Tassara, I. Ryder, C. Ledezma, G. Montalva, D. Frost, N. Sitar, R. Moss and L. Johnson (2012). Coseismic tectonic surface deformation during the 2010 Maule, Chile, M 8.8 earthquake. Earthquake Spectra, 28(S1), S39-S54.
[16] Wartman J, Dunham L, Tiwari B, Pradel D (2013) Landslides in Eastern Honshu induced by the 2011 off the Pacific Coast of Tohoku earthquake. Bull Seismol Soc Am 103(2B):1503–1521.
[17] Serva L., E. Vittori, V. Comerci, E. Esposito, L. Guerrieri, A. M. Michetti, B. Mohammadioun, G. C. Mohammadioun, S. Porfido, and R. E. Tatevossian (2016). Earthquake Hazard and the Environmental Seismic Intensity (ESI) Scale, Pure Appl. Geophys. 173(5) 1479 - 1515, doi: 10.1007/s00024-015-1177-8.
[18] Chunga K., Livio F., Mulas M., Ochoa-Cornejo, Besenzon D., Ferrario M., Michetti AM. (2018). Earthquake ground effects and intensity of the 16 April 2016, Mw 7.8 Pedernales Earthquake (Ecuador): implications for the source characterization of large subduction earthquakes. Bulletin of the Seismological Society of America 108 (6): 3384-3397, doi: 10.1785/0120180051.
[19] Xu, C., Ma, S., Tan, Z., Chao Xie I., Shinji T., Xueqiang H. (2018) Landslides triggered by the 2016 Mj 7.3 Kumamoto,Japan, earthquake. Landslides 15: 551. https://doi.org/10.1007/s10346-017-0929-1.
[20] Mato, F. and Toulkeridis, T., 2018: An unsupervised K-means based clustering method for geophysical post-earthquake diagnosis. 2017 IEEE Symposium Series on Computational Intelligence (SSCI). 1-8
[21] Serey, A., Piñero-Feliciangeli, L., Sepúlveda, S.A., Iveda F., Poblete D., Petley I., Murphy W. (2019). Landslides induced by the 2010 Chile megathrust earthquake: a comprehensive inventory and correlations with geological and seismic factors. Landslides 16: 1153. https://doi.org/10.1007/s10346-019-01150-6.
[22] Dakshanamurthy, V. &. (1973). A simple method of identifying an expansive soil. Soils and Foundations, 13(1), 97-104.
[23] CDMG. (1999). Guidelines for analyzing and mitigating liquefaction hazards. California Dept Conservation, Division of Mines, Special Publication 117, p 63.
[24] Sana, H., & Nath, S. K. (2016). Liquefaction potential analysis of the Kashmir valley alluvium, NW Himalaya. Soil Dynamics and Earthquake Engineering, 85, 11-18.
[25] Bahadori, H., Hasheminezhad, A., & Karimi, A. (2017). Development of an integrated model for seismic vulnerability assessment of residential buildings: Application to Mahabad City, Iran. Journal of Building Engineering, 12, 118-131.
[26] Cando-Jácome M., Martínez-Graña A., Chunga K., Ortíz-Hernández E. (2020). Satellite radar interferometry for assessing coseismic liquefaction in Portoviejo city, induced by the M 7.8 2016 Pedernales, Ecuador Earthquake. Environ Earth Sci 79, 467 (2020). https://doi.org/10.1007/s12665-020-09205-x.
[27] Hazen, A (1919). Hydraulic-fill dams. Transactions of the American Society of Civil Engineers, 83: 1713–1745.
[28] Seed HB, Idriss IM (1971) Simplified procedure for evaluating soil liquefaction potential. J Soil Mech Found Div ASCE 97(SM9):1249–1273.
[29] Chen CJ, Juang CH. (2000). Calibration of SPT-and CPT-based liquefaction evaluation methods. In: Mayne PW, Hryciw R, editors. Innovation sand application sin geotechnical site characterization, vol.97. Reston: Geotechnical Special Publication, ASCE; p.49–64.
[30] Juang C.H., Chen C.J., Jiang T., Andrus R.D. (2000). Risk-based liquefaction potential evaluation using standard penetration tests. Canadian Geotechnical Journal, 37 (6), pp. 1195-1208
[31] Wakamatsu, K. (1992). Evaluation of liquefaction susceptibility based on detailed geomorphological classification. In: Proceedings of the Annual Meeting of Architectural Institute of Japan, pp. 1443–1444 (in Japanese).

[32] Bray, J. D., & Luque, R. (2017). Seismic performance of a building affected by moderate liquefaction during the Christchurch earthquake. Soil Dynamics and Earthquake Engineering, 102, 99–111. https://doi.org/10.1016/j.soildyn.2017.08.011

[33] Mendoza, C., and J. W. Dewey (1984). Seismicity associated with the great Colombia–Ecuador earthquakes of 1942, 1958, and 1979: Implications for barrier models of earthquake rupture, Bull. Seismol. Soc. Am. 74, no. 2, 577–593.

[34] Ye, L., H. Kanamori, J. P. Avouac, L. Li, K. F. Cheung, and T. Lay (2016). The 16 April 2016, M 7.8 (Ms 7.5) Ecuador earthquake: A quasi-repeat of the 1942 M S 7.5 earthquake and partial re-rupture of the 1906 Ms 8.6 Colombia–Ecuador earthquake. Earth Planet. Sci. Lett. 454 248-258.

[35] Chunga, K.; Livio, F.A.; Martillo, C.; Lara-Saavedra, H.; Ferrario, M.F.; Zevallos, I.; Michetti, A.M. (2019). Landslides Triggered by the 2016 M 7.8 Pedernales, Ecuador Earthquake: Correlations with ESI-07 Intensity, Lithology, Slope and PGA-h. Geosciences, 9, 371. Doi: 10.3390/geosciences9090371.

[36] Salocchi, A.C., Minarelli, L., Lugli, S., Amoroso, S., Rollins K.M., Fontana D. (2020). Liquefaction source layer for sand blows induced by the 2016 megathrust earthquake (M 7.8) in Ecuador (Boca de Briceño). Journal of South American Earth Sciences 103, https://doi.org/10.1016/j.jsames.2020.102737.

[37] Youd TL, Perkins DH (1978) Mapping liquefaction-induced ground failure potential. J Geotech Eng Div ASCE 104(GT4):433–446.

[38] Bahadori, H., Hasheminezhad, A. (2016). Standard Penetration Test-Based Assessment of Seismic Soil Liquefaction Potential of Urmia, Iran.

[39] Bourenane, H., Bouhadad, Y., Tas, M. (2018). Liquefaction hazard mapping in the city of Boumerdès, Northern Algeria. Bull Eng Geol Environ 77(4), 1473-1489. https://doi.org/10.1007/s10064-017-1137-x

[40] Goharzay M., Noorzad A., Ahmadreza Mahboubi A., Mostafa J. (2017). A worldwide SPT-based soil liquefaction triggering analysis utilizing gene expression programming and Bayesian probabilistic method. Journal of Rock Mechanics and Geotechnical Engineering. Volume 9, Issue 4, Pages 683-693. https://doi.org/10.1016/j.jrmge.2017.03.011.

[41] Hashash, Y.M.A., Musgrove, M.I., Harmon, J.A., Groholski, D.R., Phillips, C.A., and Park, D. (2016). "DEEPSOIL 6.1, User Manual". Urbana, IL, Board of Trustees of University of Illinois at Urbana-Champaign.

[42] Lai, C.G., Bozzoni, F., Conca, D. et al. (2020) Technical guidelines for the assessment of earthquake induced liquefaction hazard at urban scale. Bulletin Earthquake Engineering.

[43] NEC-11 (2015). Norma Ecuatoriana de la Construcción. Registro Oficial No. 413 del 10 de enero de 2015. Available online: http://www.normaconstruccion.ec/ (accessed on 11 August 2020).

[44] Chunga K. (2010). Shallow crustal earthquakes and seismic zonation for Ecuador through the integration of geological, seismological and morphostructural data (in Italian). University of Insubria. Ph.D. Thesis, p. 165.

[45] Béjar-Pizarro M., Álvarez G.J., Staller A., Luna M., Pérez-López R., Monserrat O., Chunga K. (2018). InSAR-Based Mapping to Support Decision-Making after an Earthquake. Remote Sensing 10(6). DOI: 10.3390/rs10060899

[46] Pennington, W. D. (1981). Subduction of the eastern Panama Basin and seismotectonics of northwestern South America.J. Geophys. Res. B Solid Earth Planets 86(B11) 10753-10770.

[47] Hey, R. (1977). Tectonic evolution of the Cocos-Nazca spreading center. Geol. Soc. Am. Bull. 88(12) i-vi.

[48] Gutscher, M.A., Malavieille, J.S.L. and Collot, J.-Y., 1999: Tectonic segmentation of the North Andean margin: impact of the Carnegie ridge collision. Earth Planet. Sci. Lett. 168: 255–270.

[49] Aguiar, R., C. Castro, Ch. Garzón, W. Yanchatuña, L. Cumbal, and J. La Fave. (2009). Magnitud máxima en zonas fuentes para estudios de peligrosidad sísmica del Ecuador. Rev Cienc ESPE Univ Fuerzas Armadas 12 (2): 109–121.
[50] Veloza, G., R. Styron, M. Taylor and A. Mora (2012). Open-source archive of active faults for northwest South America. GSA Today 22(10) 4-10.
[51] Kelleher, J. (1972). Rupture zones of large South Amercan earthquakes and some predictions. Journal of Geophysical Research, vol 77, No. 11, pp. 2087-2103.
[52] Carena, S. (2011) - Subducting-plate topography and nucleation of great and giant earthquakes along the South America trench. Seismol. Res. Lett., 82 (5) 629-637, doi:10.1785/gssrl.82.5.629.
[53] Santibáñez, I.; Cembrano, J.; García-Pérez, T.; Costa, C.; Yáñez, G.; Marquardt, C.; Arancibia, G.; González, G. (2019). Crustal faults in the Chilean Andes: geological constraints and seismic potential. Andean Geology 46 (1): 32-65. [doi:http://dx.doi.org/10.5027/andgeoV46n1-3067].
[54] White, S. M., R. Trenkamp, and J. N. Kellogg (2003). Recent crustal deformation and the earthquake cycle along the Ecuador–Colombia subduction zone. Earth Planet. Sci. Lett. 216(3) 231-242.
[55] Chlieh M., Mothes P.A., Nocquet J.-M., Jarrin P., Charvis P., Cisneros D., Font Y., Collot J.-Y., Villegas-Lanza J.-C., Rolandone F., Vallée M., Regnier M., Segovia M., Martin X., Yepes H. (2014). Distribution of discrete seismic asperities and aseismic slip along the Ecuadorian megathrust. Earth Planet. Sci. Lett. 400, 292_301.
[56] Nocquet, J. M., P. Jarrin, M. Vallée, P. A. Mothes, R. Grandin, F. Rolandone, B. Delouis, H. Yepes, Y. Font, D. Fuentes, M. Régnier, A. Laurendeau, D. Cisneros, S. Hernandez, A. Sladen, J.-C. Singaucho, H. Mora, J. Gomez, L. Montes, and P. Charvis (2016). Supercycle at the Ecuadorian subduction zone revealed after the 2016 Pedernales earthquake. Nat Geosci. 10(2) 145-149.
[57] IOC Intergovernmental Oceanographic Commission (2020) Tsunami sources, hazards, risk and uncertainties associated with the Colombia-Ecuador Subduction Zone. Guayaquil, Ecuador, 27–29 January. Paris, UNESCO.
[58] Toulkeridis, T., Chunga, K., Rentería, W., Rodriguez, F., Mato, F., Nikolaou, S., Cruz D´Howitt, M., Besenzon, D., Ruiz, H., Parra, H. and Vera-Grunauer, X. (2017). The 7.8 M Earthquake and Tsunami of the 16th April 2016 in Ecuador - Seismic evaluation, geological field survey and economic implications. Science of tsunami hazards, 36: 197-242.
[59] Kanamori, H. and McNally, K. (1982). Variable rupture mode of the suduction zone along the Ecuador-Colombia coast. Bull. Seismol. Soc. Am. 72, 1241_1253.
[60] Yoshimoto M. Kumagai H., Acero W., Ponce G., Vasconez F., Arrais S., Ruiz M., Alvarado A., Pedraza Garcia P., Dionicio V., Chamorro O, Maeda Y., Nakano M. (2017). Depth dependent rupture mode along the Ecuador-Colombia subduction zone. Geophysical Research Letters. 44, 2203-2210. Doi: 10.1002/2016GL071929.
[61] Pulido N., Yoshimoto M., Sarabia A.M. (2020). Broadband wavelength slip model of the 1906 Ecuador-Colombia megathrust-earthquake based on seismic intensity and tsunami data. Tectonophysics. Volume 774, https://doi.org/10.1016/j.tecto.2019.228226
[62] Michaud François, Witt C., Royer J.Y. (2009). Influence of the subduction of the Carnegie volcanic ridge on Ecuadorian geology : reality and fiction. In : Mahlburg Kay S. (ed.), Ramos V. (ed.), Dickinson W. (ed.) Backbone of the Americas : Shallow Subduction, Plateau Uplift, and Ridge and Terrane Collision. Boulder : The Geological Society of America, (204), 217-228. (Memoir - Geological Society of America ; 204). ISBN 978-0-8137-1204-8.
[63] Blanco-Chao R., K. Pedoja, C. Witt, J. Martinod, L. Husson, V. Regard, L. Audin, M. Nexer, B.C., Delcaillau, M. Saillard, D. Melnick, J. F. Dumont, E. Santana, E. Navarrete, C. Martillo, M., Pappalardo, L. Ayala, J. F. Araya, A. Feal-Pérez, D. Correa and I. Arozarena-Llopis.

(2014). Chapter 10 The rock coast of South and Central America. Geological Society, London, Memoirs, v.40; p155-191. doi: 10.1144/M40.10.

[64] Pedoja, K., Dumont, J. F., Lamothe, M., Ortlieb, L., Collot, J.-Y., Ghaleb, B., Auclair, M., Alvarez, V., Labrousse B. (2006). Plio-Quaternary uplift of the Manta Peninsula and La Plata Island and the subduction of the Carnegie Ridge, central coast of Ecuador. J. S. Am. Earth Sci. 22(1) 1-21.

[65] Graindorge, D., A. Calahorrano, P. Charvis, J.Y Collot, and N. Bethoux (2004), Deep structures of the Ecuador convergent margin and the Carnegie Ridge, possible consequence on great earthquakes recurrence interval, Geophys. Res. Lett., 31, L04603, doi:10.1029/2003GL018803.

[66] Font Y., Segovia, M., Vaca, S., Theunissen T. (2013). Seismicity patterns along the Ecuadorian subduction zone: new constraints from earthquake location in a 3-D a priori velocity model. Geophys. J. Int., 193, pp. 263-286, 10.1093/gji/ggs083

[67] Nocquet, J. M., J. C. Villegas-Lanza, M. Chlieh, P. A. Mothes, F. Rolandone, P. Jarrin, D. Cisneros, A. Alvarado, L. Audin, F. Bondoux, et al. (2014). Motion of continental slivers and creeping subduction in the northern Andes, Nature Geosci. 7, no. 4, 287–291.

[68] Alvarado, A., L. Audin, J. M. Nocquet, E. Jaillard, E., P. Mothes, P. Jarrín, M. Segovia, F. Rolandone, and D. Cisneros (2016). Partitioning of oblique convergence in the Northern Andes subduction zone: Migration history and the present-day boundary of the North Andean Sliver in Ecuador. Tectonics 35(5) 1048-1065.

[69] Marcaillou, B., J. Y. Collot, A. Ribodetti, E. d'Acremont, A. A. Mahamat, and A. Alvarado (2016). Seamount subduction at the North-Ecuadorian convergent margin: Effects on structures, inter-seismic coupling and seismogenesis. Earth Planet. Sci. Lett. 433 146-158.

[70] Collot, J. Y., E. Sanclemente, J. M. Nocquet, A. Leprêtre, A. Ribodetti, P. Jarrin, M. Chlieh, D. Graindorges, and P. Charvis (2017). Subducted oceanic relief locks the shallow megathrust in central Ecuador, J. Geophys. Res. B Solid Earth Planets 122 3286–3305, doi:10.1002/2016JB013849.

[71] IGEPN. Instituto Geofísico Escuela Politécnica Nacional. Quito. Available online: http://www.igepn.edu.ec/solicitud-de-datos (accessed on 20 May 2020).

[72] Beauvalet C., Marinière, J., Yepes, H., Audin, L., Nocquet, J.M., Alvarado, A., Baize, S., Aguilar, J., Singaucho, J.C., Jomard, H.A. (2018). New Seismic Hazard Model for Ecuador. Bull. Seismol. Soc. Am. 2018, 108, 1443–1464. [CrossRef]

[73] Wells, D.L.; Coppersmith, K.J. 1994. New empirical relationships among magnitude, rupture length, rupture width, rupture area, and surface displacement. Bulletin of the Seismological Society of America 84: 974-1002.

[74] Wesnousky, 2008. Displacement and geometrical characteristics of earthquake surface ruptures: issues and implications for seismic-hazard analysis and the process of earthquake rupture. Bulletin of the Seismological Society of America 98 (4): 1609-1632. doi: 10.1785/0120070111.

[75] Stirling, M.; Goded, T.; Berryman, K.; Litchfield, N. 2013. Selection of earthquake scaling relationships for seismic-hazard analysis. Bulletin of the Seismological Society of America 103 (6): 2993-3011. doi: 10.1785/0120130052.

[76] INEC (2010). Base de Datos – Censo de Población y Vivienda del Ecuador. Disponible en: http://www.ecuadorencifras.gob.ec/base-de-datos-censo-de-poblacion-y-vivienda/.

[77] Stay-Coello, Villa P., Gomez de la Torre, M, Briones M. (2018). Determinación de zonas de peligrosidad Sísmica en la cuenca del río Jama con el uso de perfiles de respuesta del suelo. Journal of science and research: e-issn: 2528-8083, vol. 3, No. icce 2018, pp. 74-80. https://doi.org/10.26910/issn.2528-8083vol3issICCE2018.2018pp90-98p.

[78] Leonard, M. 2010. Earthquake fault scaling: Self consistent relating of rupture length width, average displacement, and moment release. Bulletin of the Seismological Society of America 100 (5A): 1971-1988.

[79] Fukushima, Y.; Tanaka, T. 1990. A New Attenuation Relation for Peak Horizontal Acceleration of Strong Earthquake Ground Motion in Japan. Bulletin of the Seismological Society of America 80 (4): 757-783.

[80] Chunga K. (2019). Reconocimiento geológico de la ciudad de Jama. Microzonificación sísmica de ciudades prioritarias de la costa ecuatoriana de conformidad con los requisitos de la norma ecuatoriana de la construcción NEC. Universidad de los Andes, Proyecto BID # EC-T1354. Reporte técnico 34 pág.

[81] Daza J., Trstancho J., Caicedo B. (2019). Caracterización geotécnica y geofísica de la ciudad de Jama. Microzonificación sísmica de ciudades prioritarias de la costa ecuatoriana de conformidad con los requisitos de la norma ecuatoriana de la construcción NEC. Universidad de los Andes, Proyecto BID # EC-T1354. Reporte técnico 94 pág.

[82] Wang, W (1979). Some Findings in Soil Liquefaction. Report Water Conservancy and Hydro-electric Power Scientific Research Institute, Beijing, China, 1-17.

[83] Seed HB, Tokimatsu K, Harder LF, Chung RM (1985) The influence of SPT procedures in soil liquefaction resistance evaluations. J GeotechEng Div ASCE 111(12):1425–1445.

[84] Stainforth, R. M. (1948). Applied micropaleontology in coastal Ecuador. Journal of Paleontology, 616 113-151.

[85] Whittaker J.E. Benthic Cenozoic Foraminifera from Ecuador. Taxonomy and distribution of smaller benthic Foraminifera from coastal Ecuador (late Oligocene – Late Pliocene). British Museum (Nature History) publ., 1988; 194 p., London.

[86] Kramer, S.L. (1996) Geotechnical Earthquake Engineering. Prentice-Hall, New Jersey.

[87] Osorio Gutiérrez, B. (2009).Resistencia Estática y Cíclica de Relaves Integrales. Disponible en http://repositorio.uchile.cl/handle/2250/103414.

[88] Garcia, J., G. Weatherhill, M. Pagani, L. Rodriguez, V. Poggi, and the SARA Hazard Working Group 517 (2017). Building an open seismic hazard model for South America: The SARA-PSHA model, 16th World Conference on Earthquake Engineering, Santiago, Chile, 9–13 January, Paper Number 2145, 13 pp.

[89] Parra, H., M. Benito, and J. Gaspar-Escribano (2016). "Seismic Hazard Assessment in Continental Ecuador." Bulletin of Earthquake Engineering 14 (8): 2129–2159. doi:10.1007/s10518-016-583 9906-7.

[90] Seed RB, Cetin KO, Moss RES, Kammerer AM, Wu J, Pestana JM, Riemer MF, Sancio RB, Bray JD, Kayen RE, Faris A (2003). Recent advances in soil liquefaction engineering: a unified and consistent framework. In: Proceedings of 26th annual ASCE L.A. Geotechnical Spring Seminar, Long Beach, p 71

[91] Seed, H.B., and Idriss, I.M. (1982). Ground Motions and Soil Liquefaction During earthquakes. Earthquake Engineering Research Institute Monograph.

[92] Seed HB, T. K. (1985). The influence of SPT procedures in soil liquefaction resistance evaluations. J GeotechEng Div ASCE 111(12), 1425–1445.

[93] Juang C. H., Yuan H., Lee D-H., Lin, P. S. (2003). Simplified cone penetration test-based method for evaluating liquefaction resistance of soils. Journal of Geotechnical and Geoenvironmental Engineering, 129(1), 66-80. https://doi.org/10.1061/(ASCE)1090-0241(2003)129:1(66)

[94] Youd, T. L., and Idriss, I. M., eds. (1997). Proc., NCEER Workshop on Evaluation of liquefaction Resistance of Soils, Nat. Ctr. for Earthquake Engrg. Res., State Univ. of New York at Buffalo.

[95] Youd T.L., Idriss I.M. (2001). Liquefaction Resistance of Soils: Summary Report from the 1996 NCEER and 1998 NCEER/NSF Workshops on Evaluation of Liquefaction Resistance of Soils. Journal of Geotechnical and Geoenvironmental Engineering, Volume 127, Issue 4, https://doi.org/10.1061/(ASCE)1090-0241(2001)127:4(297)

[96] Liao S, Whitman. R. (1986). Overburden correction factor for SPT in sand. J Geotech Eng ASCE, 112(3):373–377.

[97] Youd TL, Idriss IM, Andrus RD, Arango I, Castro G, Christian TV, Dobry R, Finn WDL, Harder LF, Hynes ME, Ishihara K, Koester JP, Liao SSC,MarcursonWF III,Marti GR, Mitchell JK, Moriwaki Y, Power MS, Robertson PK, Seed RB, Stokoe KH II (2001). Liquefaction resistance of soils: summary report from the 1996 NCEER and 1998 NCEER/NSF workshops on evaluation of liquefaction resistance of soils. J Geotech Geoenviron Eng ASCE 127(10):817–833.

[98] Iwasaki T, T. K. (1982). Microzonation for soil liquefaction potential using simplified methods. Procrd International Conference on microzonation, 3:1310–1330.

[99] Baldock, J. W. (1985). The Northern Andes: a review of the Ecuadorian Pacific margin. In The Ocean Basins and Margins (pp. 181-217). Springer, Boston, MA.

[100] Proust, J. N., Martillo, C., Michaud, F., Collot, J. Y., & Dauteuil, O. (2016). Subduction of seafloor asperities revealed by a detailed stratigraphic analysis of the active margin shelf sediments of Central Ecuador. Marine Geology, 380, 345-362.

[101] Lee, J.-C., H.-T. Chu, J. Angelier, Y.-C. Chan, J.-C. Hu, C.-Y. Lu, and R.-J.Rau (2002), Geometry and structure of northern surface ruptures of the1999,M= 7.6 Chi-Chi Taiwan earthquake: Influence from inherited foldbelt structures,J. Struct. Geol.,24, 173–192.

[102] Romeo, R., & Pugliese, A. (2000). Seismicity, seismotectonics and seismic hazard of Italy. Engineering geology, 55(4), 241-266.

[103] Douglas, J. (2003). Earthquake ground motion estimation using strong-motion records: a review of equations for the estimation of peak ground acceleration and response spectral ordinates. Earth-Science Reviews, 61(1-2), 43-104.

[104] Ambraseys, N. N., Douglas, J., Sarma, S. K., & Smit, P. M. (2005). Equations for the estimation of strong ground motions from shallow crustal earthquakes using data from Europe and the Middle East: horizontal peak ground acceleration and spectral acceleration. Bulletin of earthquake engineering, 3(1), 1-53.

[105] Schnabel, P.B., Lysmer, J. and Seed, H.B., 1972, SHAKE - A computer program for earthquake analysis of horizontally layered sites, Earthquake Engineering Research Center, University of California, Berkeley, Report No. EERC 72-12.

[106] Vucetic, M. and Dobry, R. (1991) “Effect of soil plasticity on cyclic response.” Journal of Geotechnical Engineering, 117(1), 89–107.

Supplementary Document

Seismically induced soil liquefaction and geological conditions in the city of Jama due to the Mw7.8 Pedernales earthquake in 2016, NW Ecuador

Diego Aviles-Campoverde[1], Kervin Chunga[2], Eduardo Ortiz-Hernández[2-3], Eduardo Vivas-Espinoza[1], Theofilos Toulkeridis[4], Gabriela Morales-Delgado[1], Dolly Delgado-Toala[5]

Facultad de Ingeniería en Ciencias de la Tierra, Escuela Superior Politécnica del Litoral, Campus Gustavo Galindo Km 30.5 Vía Perimetral, P.O. Box 09-01-5863, Guayaquil, Ecuador. E-mail: daaviles@espol.edu.ec; eevivas@espol.edu.ec; amorales@espol.edu.ec

Departamento de Construcciones Civiles, Facultad de Ciencias Matemáticas, Físicas y Químicas. Universidad Técnica de Manabí, UTM, Av. José María Urbina, Portoviejo 130111, Ecuador. E-mail: kervin.chunga@utm.edu.ec; eduardo.ortiz@utm.edu.ec

Department of Civil Engineering, University of Alicante, 03690 Alicante, Spain

Universidad de las Fuerzas Armadas ESPE, Av. Gral. Rumiñahui s/n, P.O.BOX 171-5-231B, Sangolquí, Ecuador. E-mail: ttoulkeridis@espe.edu.ec

Facultad de ingeniería, Universidad Laica Eloy Alfaro de Manabí, Ciudadela universitaria, vía San Mateo, Manta, Ecuador. E-mail: dolly.delgado@uleam.edu.ec

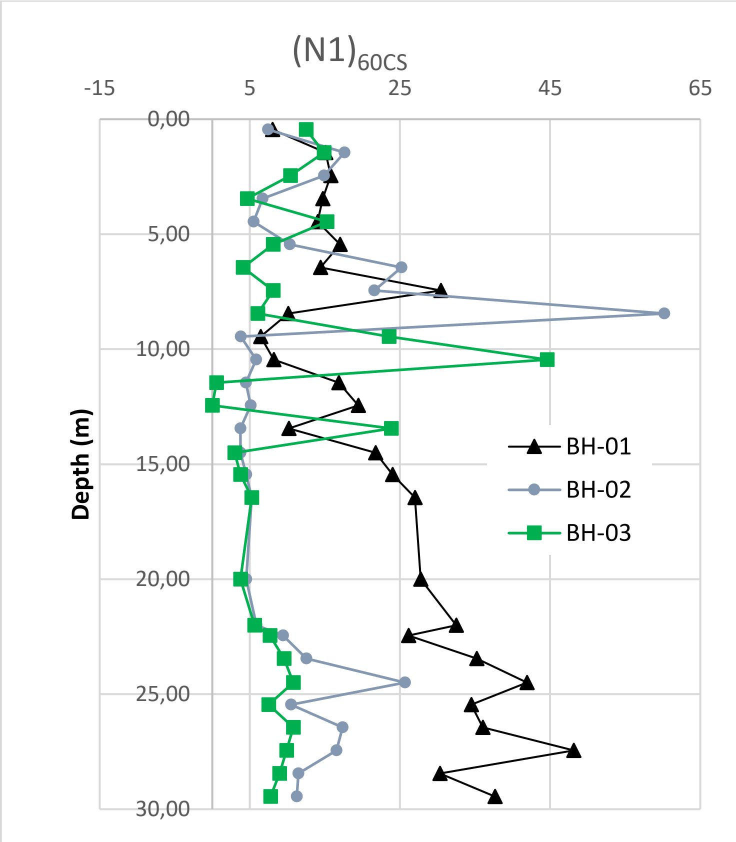

Figure 1.- SPT test results vs depth

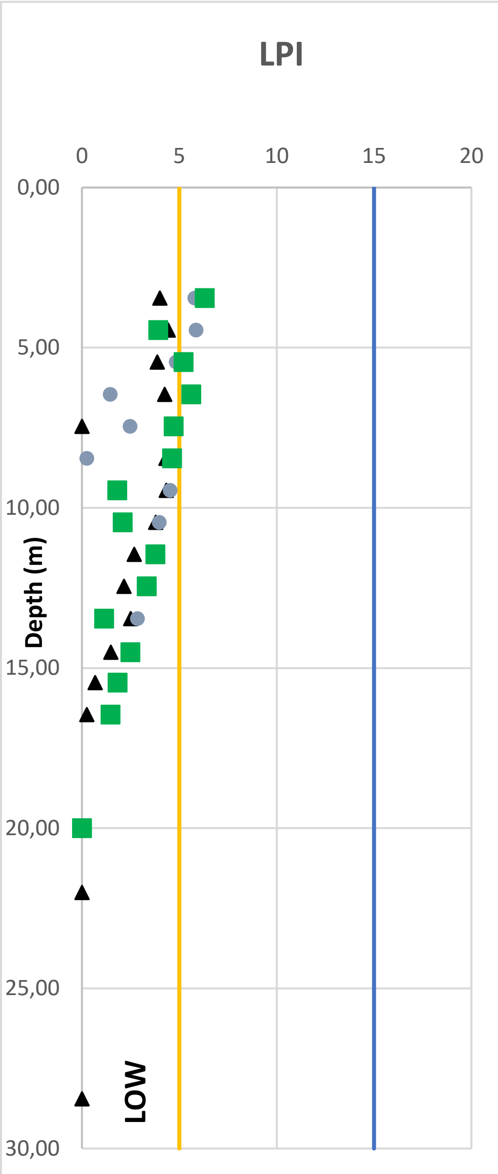

Figure 2.- Results of the liquefaction potential index (LPI)

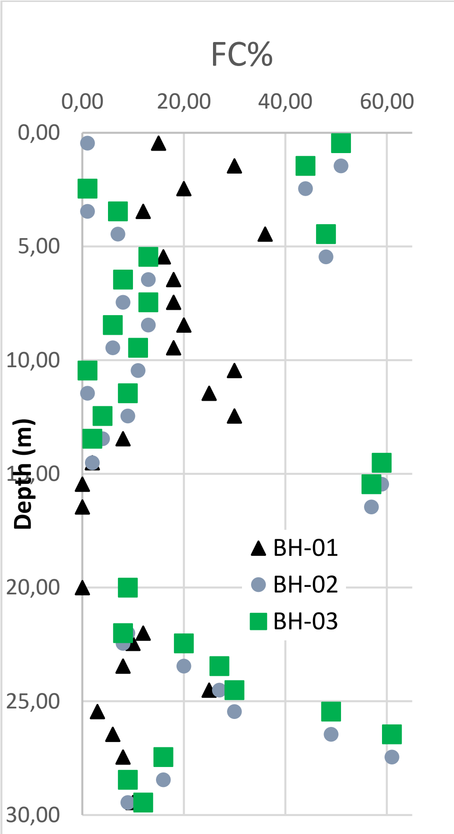

Figure 3.- Fine content

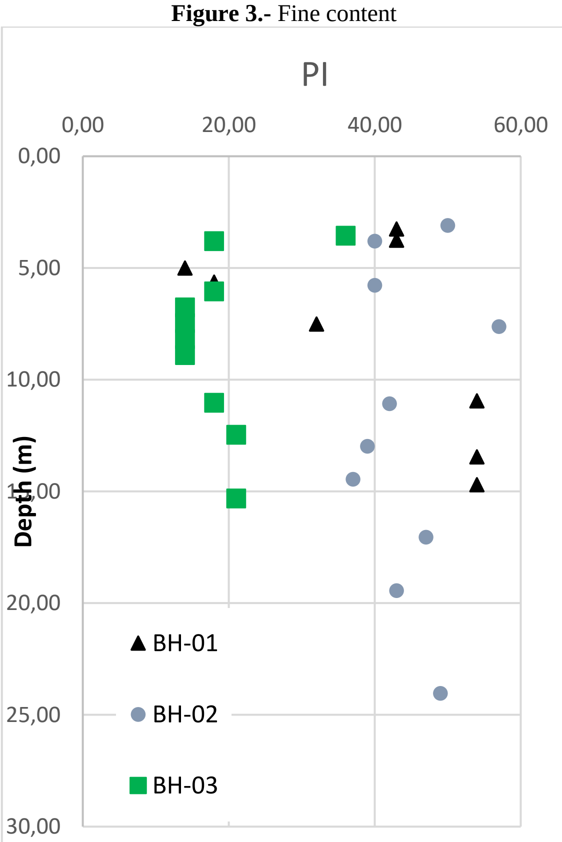

Figure 4.- Plastic Index

Table 1.- LSN results

BH	LPI	LSN
BH-01	7.12	82.48
BH-02	28.30	122.68
BH-03	29.65	142.20

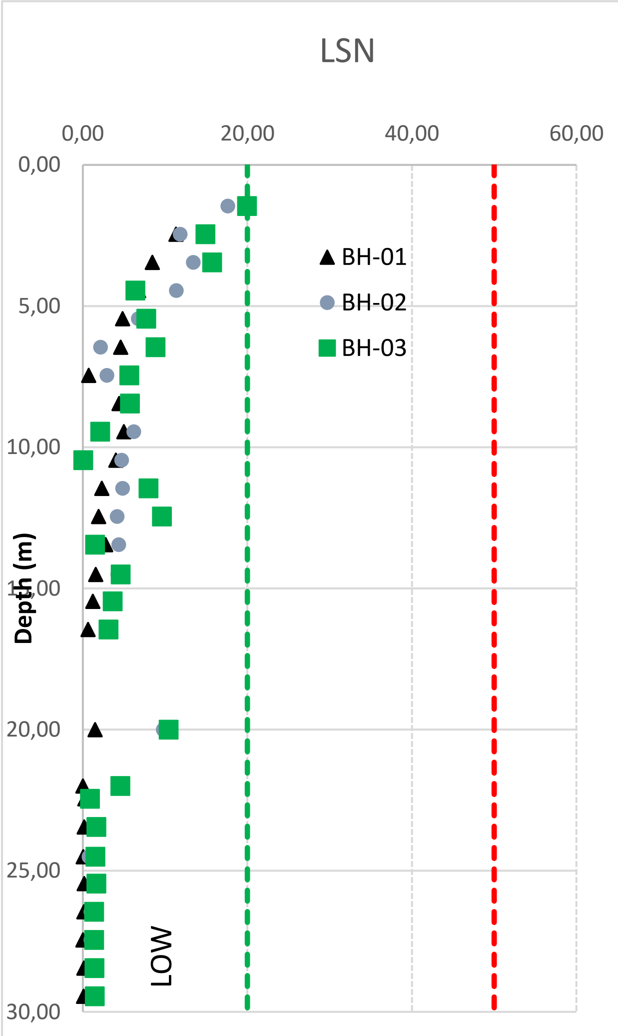

Figure 5.- LSN chart

Mov	Scale Factor	Event	Magnitude	Fault Type	R_JB (Km)	R_rup (Km)	Vs30 (m/s)	File Name
1	1.1482	Chichi, Taiwan, 1999	7.62	Reverse Oblique	9.62	9.62	427.73	CHICHI_CHY024
2	1.1646	Chichi, Taiwan, 1999	7.62	Reverse Oblique	16.04	16.04	233.14	CHICHI_CHY036
3	2.1396	Chichi, Taiwan, 1999	7.62	Reverse Oblique	24.1	24.1	442.15	CHICHI_CHY046
4	1.8878	Chichi, Taiwan, 1999	7.62	Reverse Oblique	24.13	24.13	169.52	CHICHI_CHY047
5	2.0297	Chichi, Taiwan, 1999	7.62	Reverse Oblique	37.48	37.48	318.52	CHICHI_CHY088
6	1.5388	Chichi, Taiwan, 1999	7.62	Reverse Oblique	40.88	40.88	423.4	CHICHI_CHY033
7	1.5063	Chichi, Taiwan, 1999	7.62	Reverse Oblique	35.68	35.68	393.77	CHICHI_TCU034
8	1.3811	Chichi, Taiwan, 1999	7.62	Reverse Oblique	7.64	7.64	350.06	CHICHI_TCU051
9	1.2063	Chichi, Taiwan, 1999	7.62	Reverse Oblique	6.34	6.34	359.13	CHICHI_TCU055
10	1.2581	Chichi, Taiwan, 1999	7.62	Reverse Oblique	2.11	2.11	389.41	CHICHI_TCU101

Table 2.- Seismological characteristics of the selected seismic movements compatible with the target Spectrum

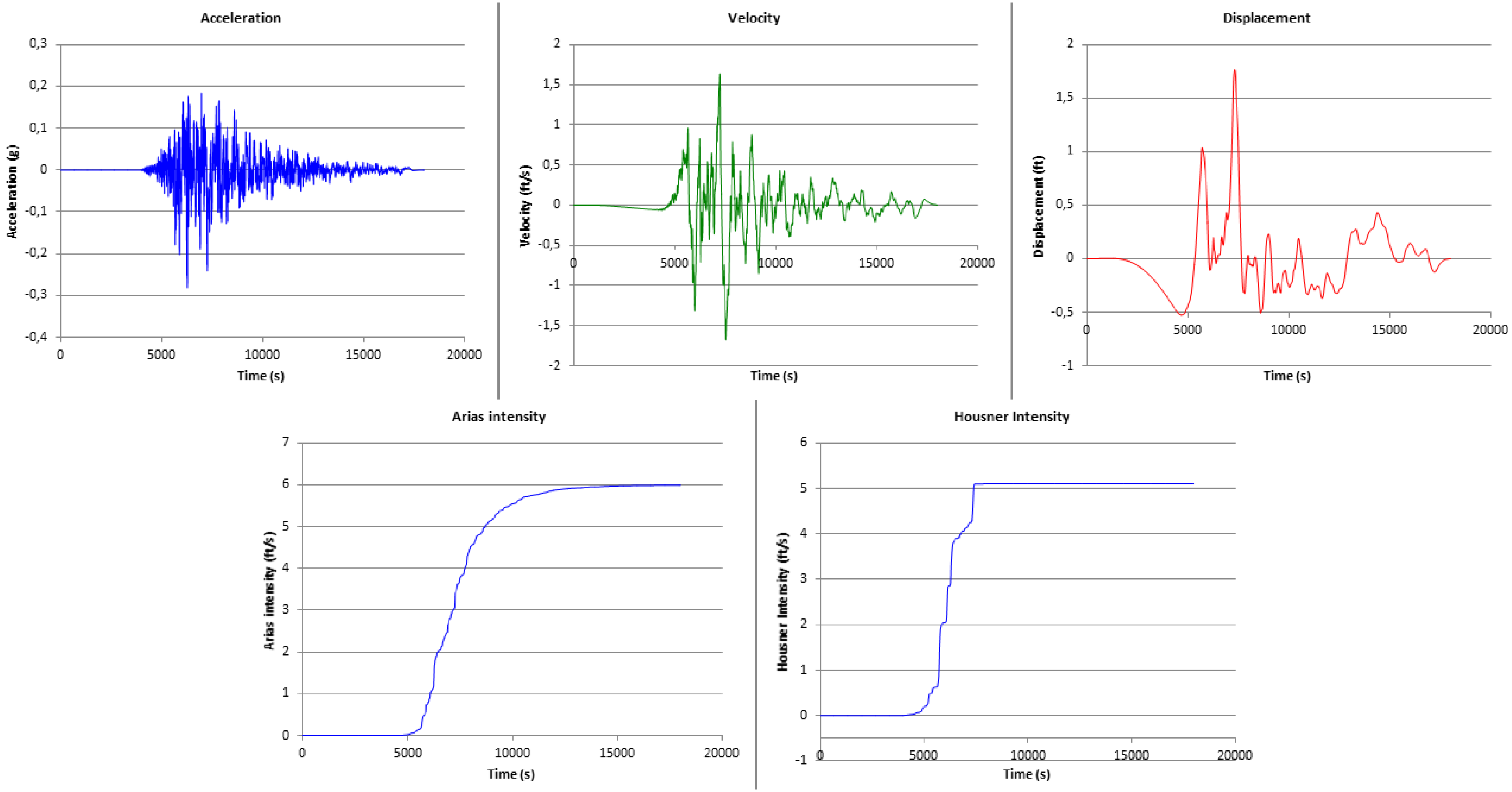

Figure 6.- Records time-history and dynamic parameters of one of the earthquakes considered for the analysis corresponding to 475 years of return period (PEER, Center for the Development of Seismic Engineering of the Pacific).

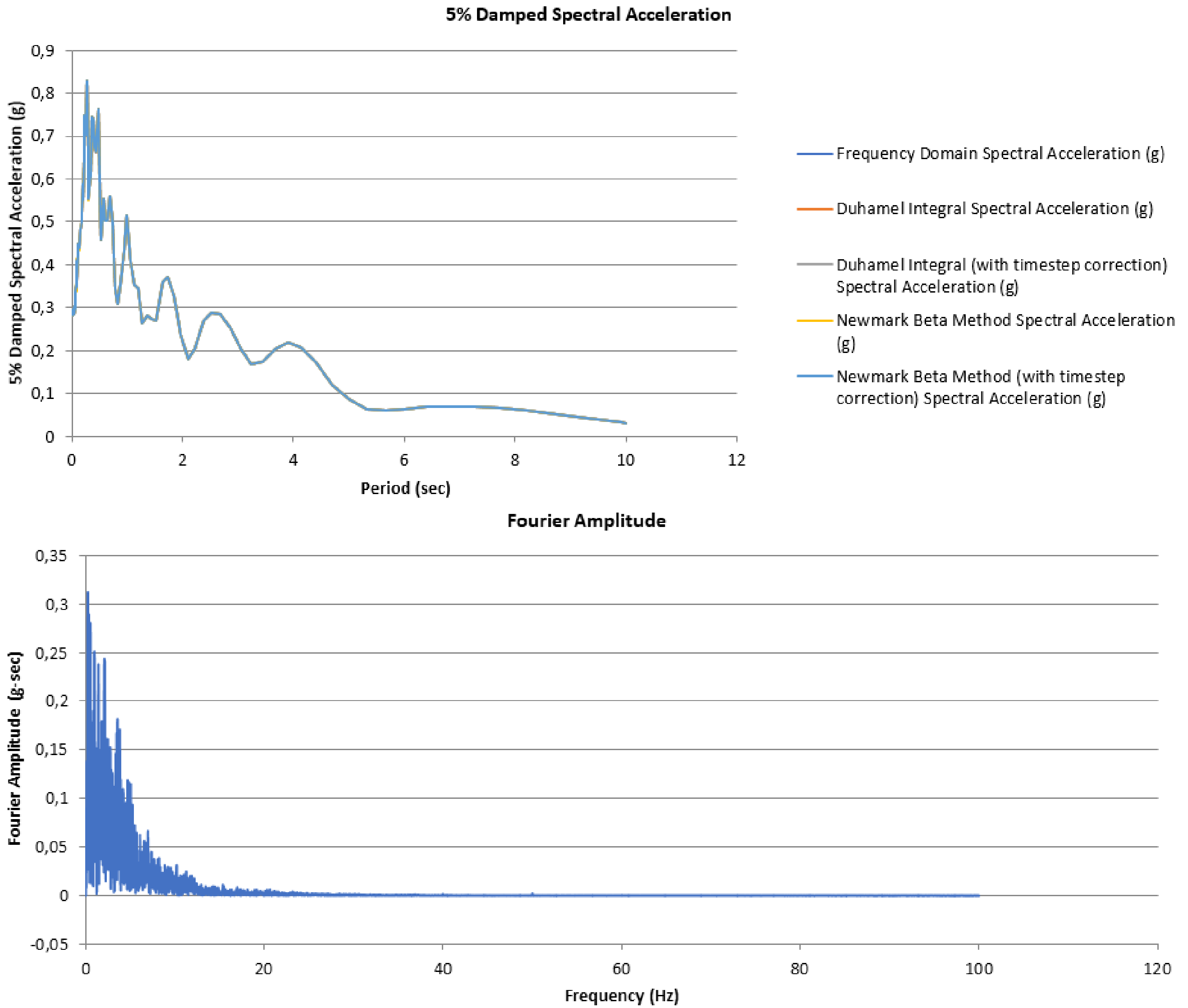

Figure 7.- Dynamic parameters of one of the earthquakes considered for the analysis corresponding to 475 years of return period (PEER, Center for the Development of Seismic Engineering of the Pacific).

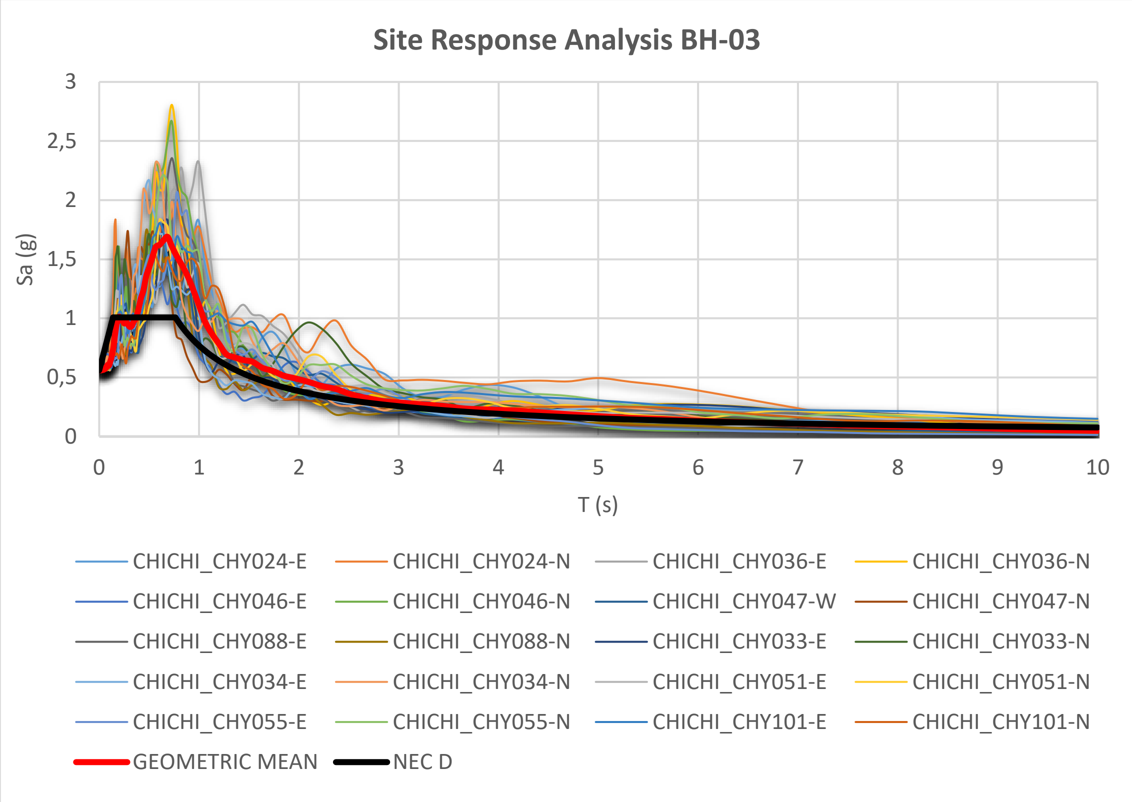

Figure 8.- Comparison of acceleration spectra for the 5% structural damping for the horizontal components of the 10 earthquakes for coluvial deposits (ie. BH-03).

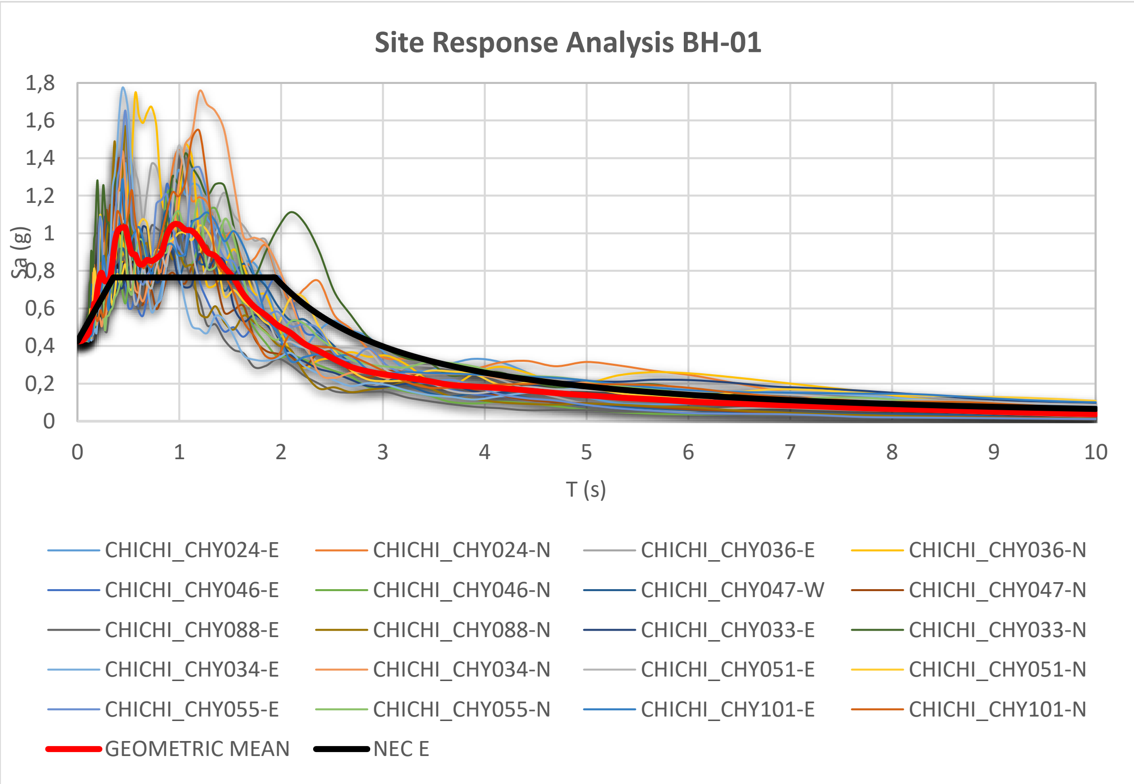

Figure 9.- Comparison of acceleration spectra for the 5% structural damping for the horizontal components of the 10 earthquakes for alluvial soils (ie., BH-01).

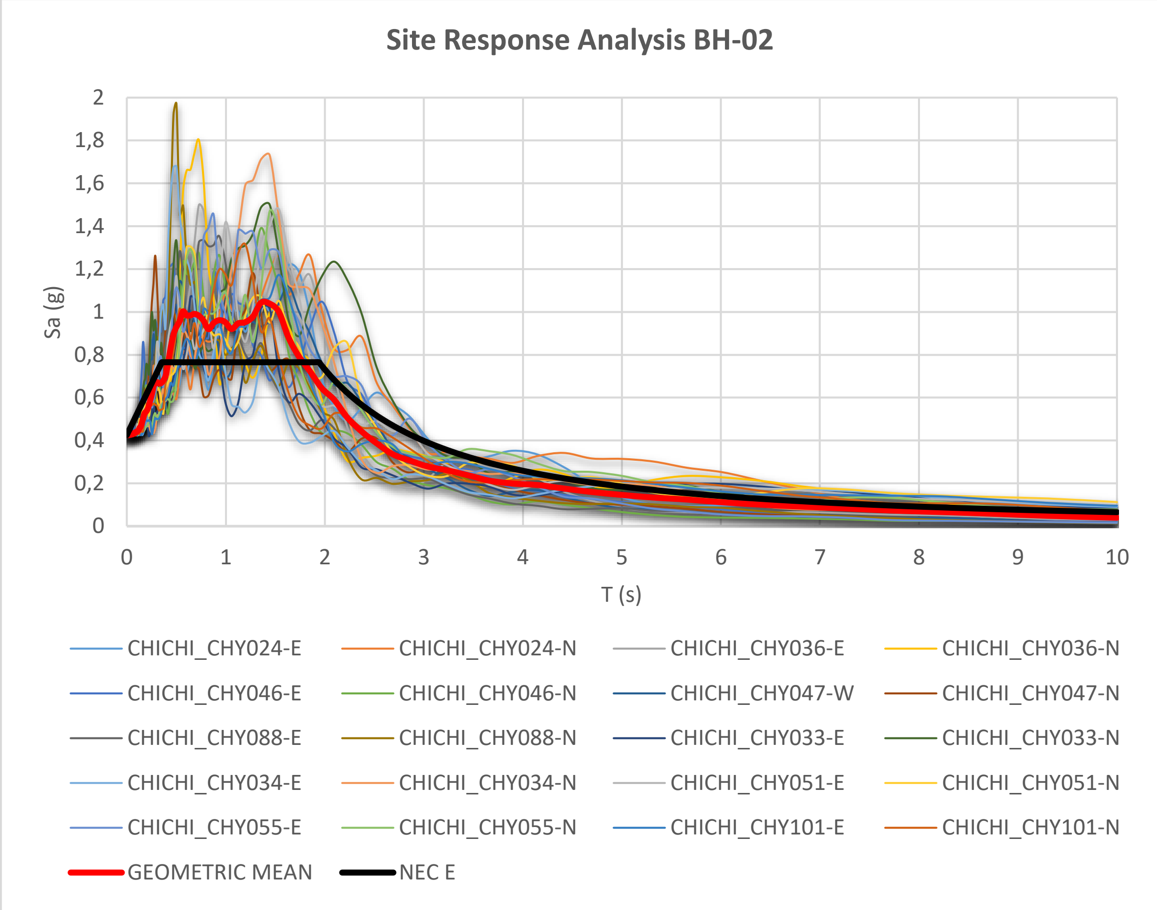

Figure 10.- Comparison of acceleration spectra for the 5% structural damping for the horizontal components of the 10 earthquakes for abandonated flooplain deposits (ie., BH-02)

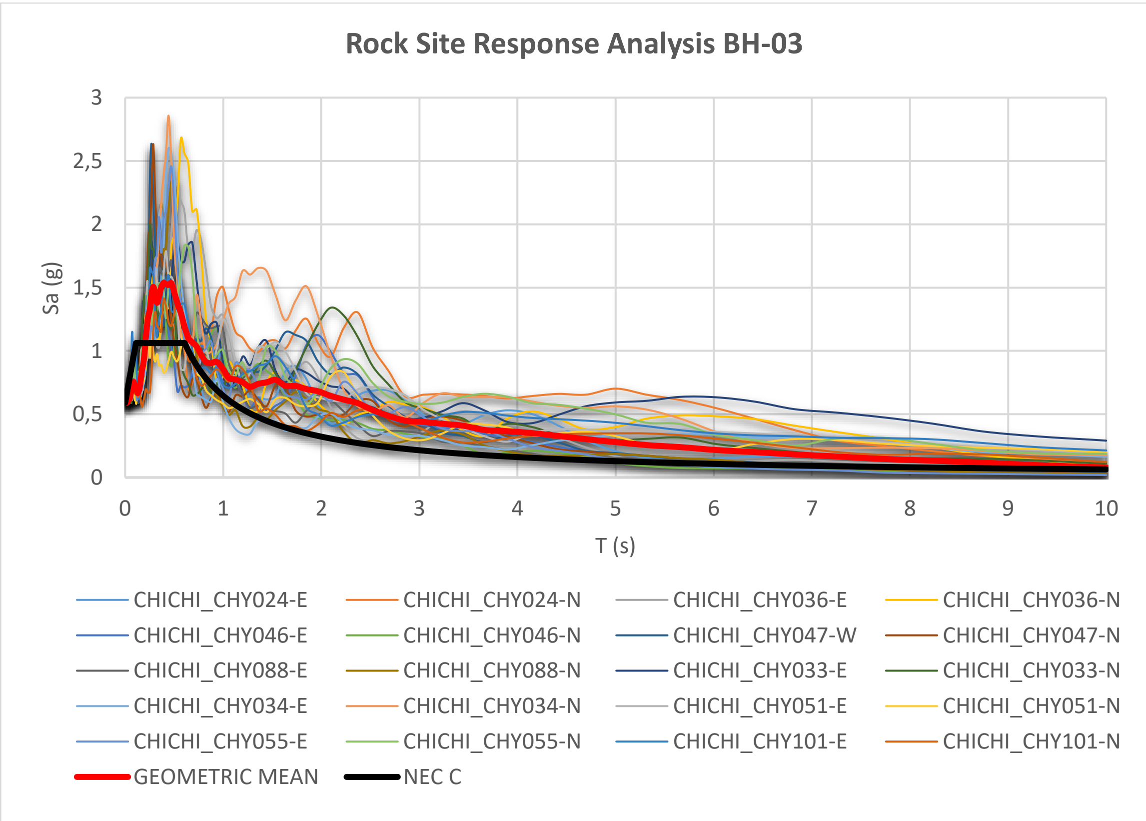

Figure 11.- Rock response spectrum for JA-BH-03 and comparison with NEC C spectrum

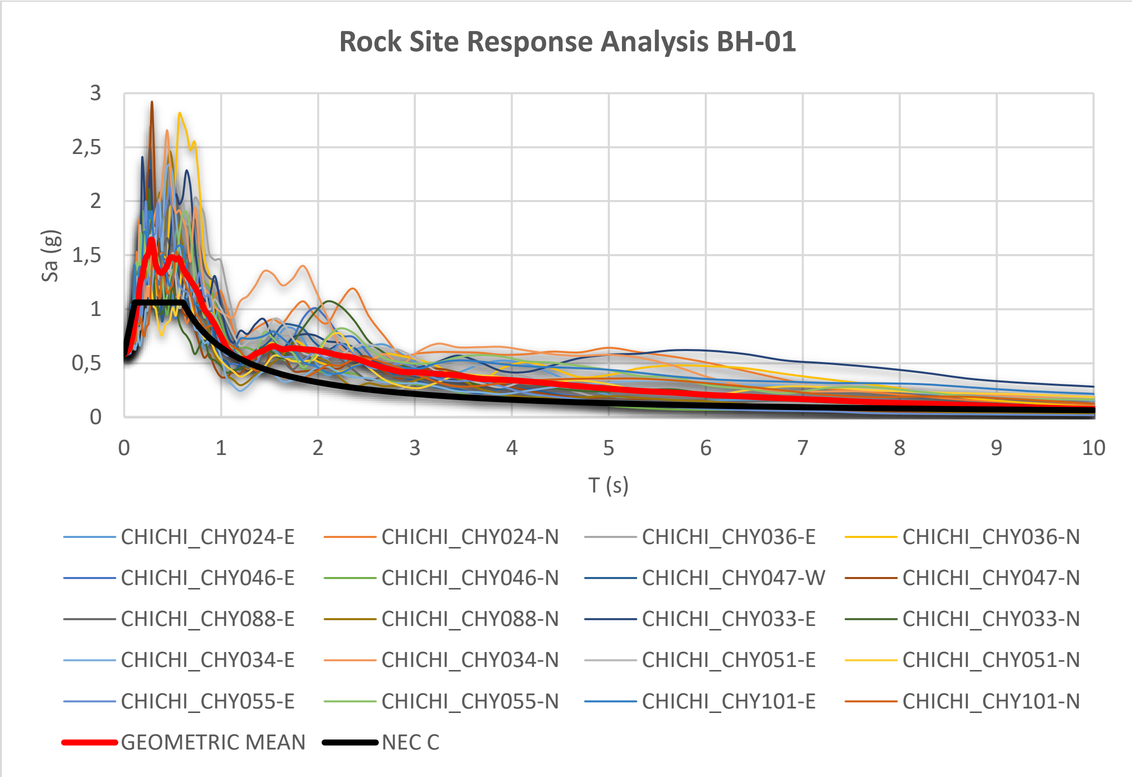

Figure 12.- Rock response spectrum for BH-01 and comparison with NEC C spectrum

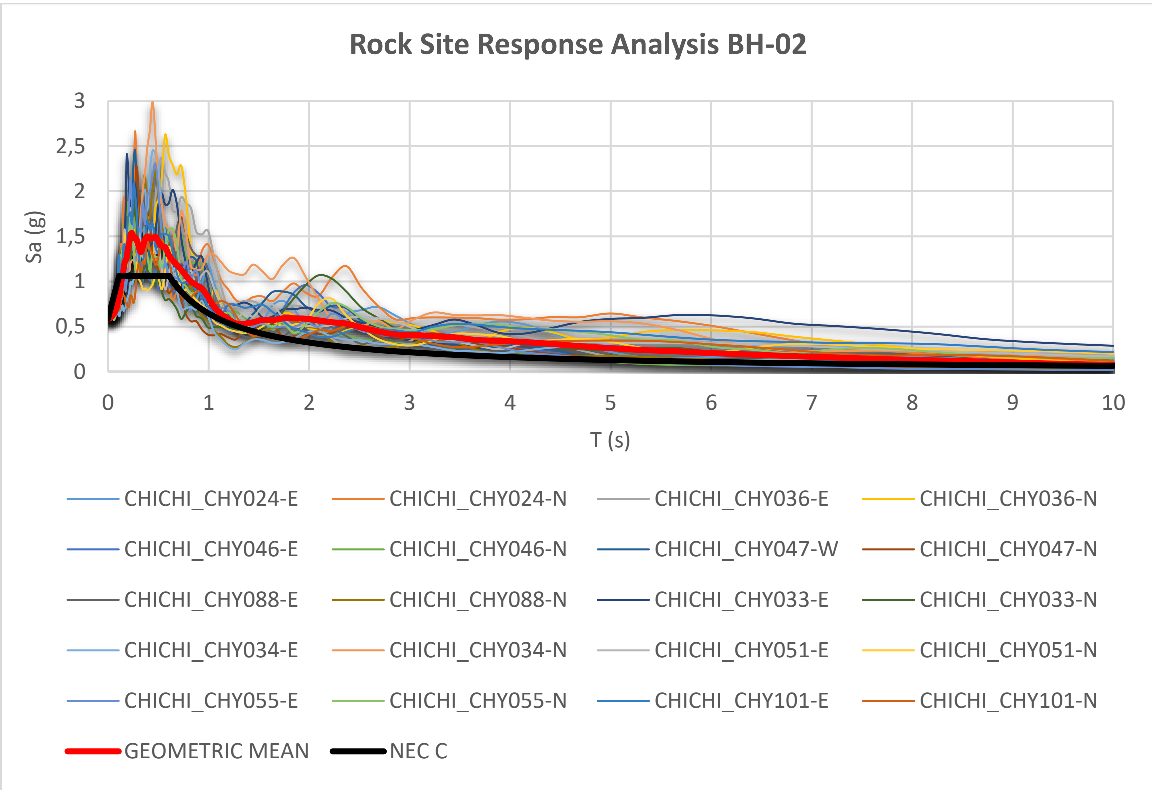

Figure 13.- Rock response spectrum for BH-02 and comparison with NEC C spectrum

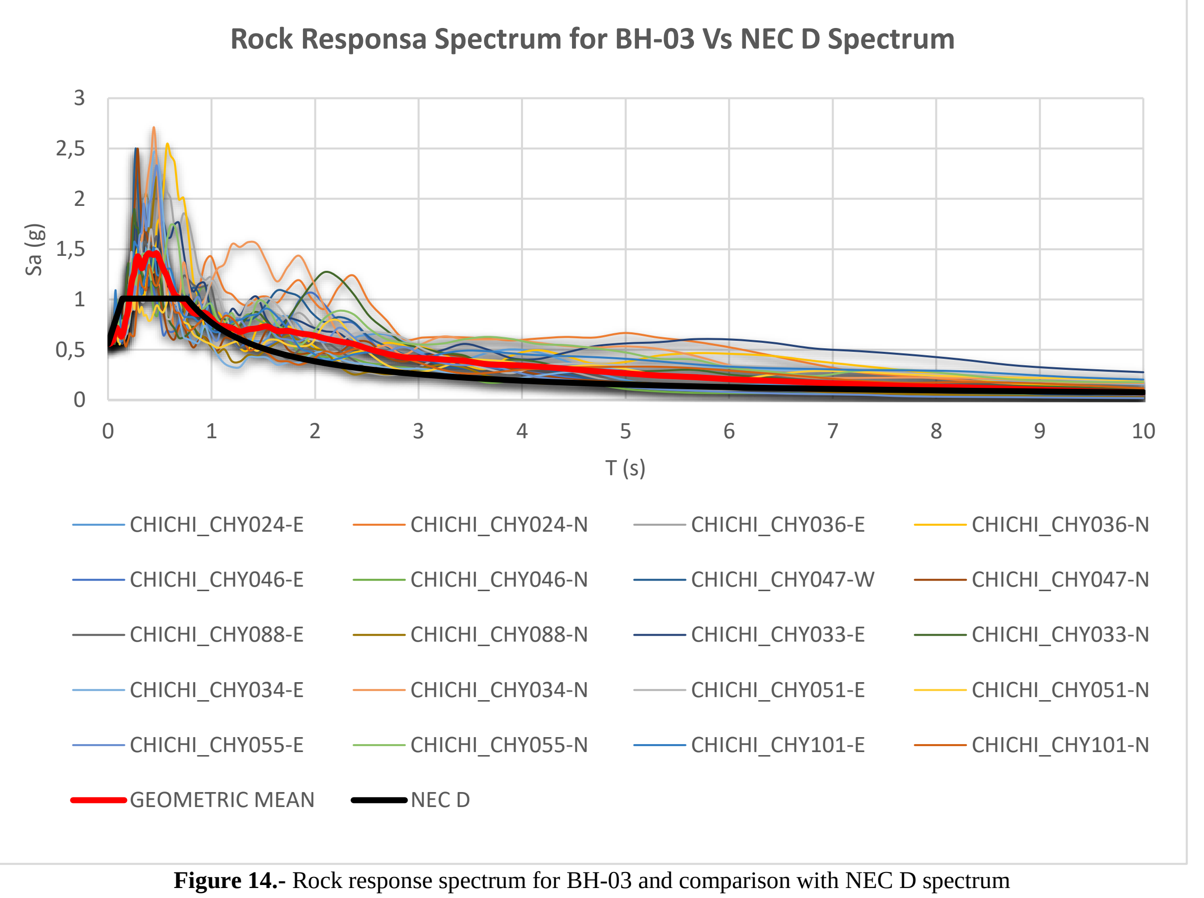

Figure 14.- Rock response spectrum for BH-03 and comparison with NEC D spectrum

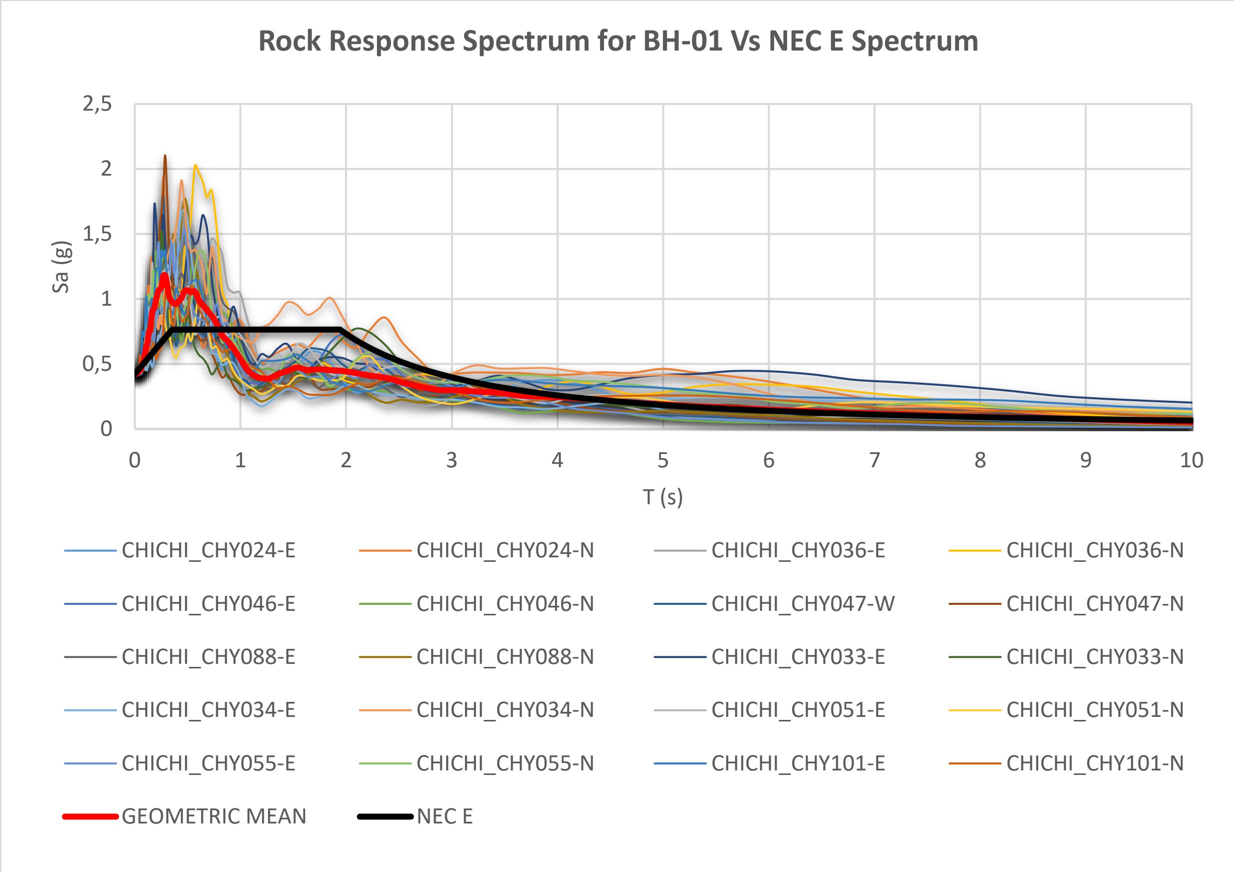

Figure 15.- Rock response spectrum for BH-01 and comparison with NEC E spectrum

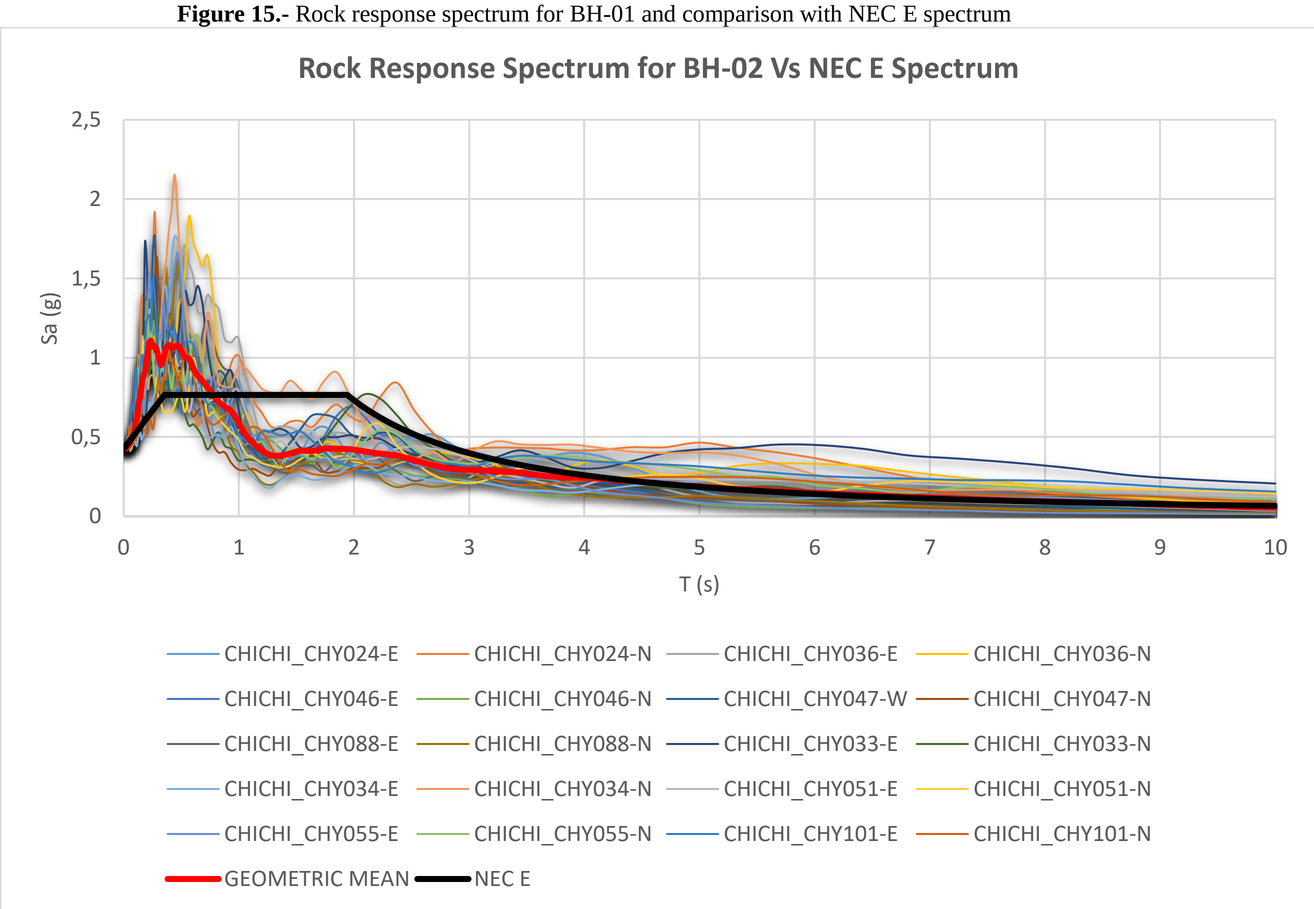

Figure 16.- Rock response spectrum for BH-02 and comparison with NEC E spectrum

Layer	Type	Thickness	ϒ	V_s	IP	σ'_{vo}	S_u	OCR	k_0
1.00	CH	3.25	15.25	157.73	43.00	24.78	56.31	11.47	0.62
2.00	CH	0.50	15.25	157.73	43.00	50.92	56.31	4.11	0.62
3.00	MH	1.25	15.25	157.73	43.00	55.68	56.31	3.62	0.62
4.00	MH	0.63	15.25	157.73	43.00	60.79	56.31	3.19	0.62
5.00	ML	1.88	15.25	157.73		67.62			0.44
6.00	MH	3.44	15.25	157.73	56.00	82.09	56.31	2.08	0.68
7.00	ML	2.50	15.25	157.73		98.25			0.44
8.00	ML	1.25	15.25	157.73		108.45			0.44
9.00	Sandstone	1.56	19.64	437.79		119.51			0.44
10.00	Conglomerate	2.50	19.64	437.79		139.47			0.44
11.00	Lutites	1.56	19.64	437.79		159.42			0.44
12.00	Lutites	3.13	19.64	437.79		182.47			0.44
13.00	ML	1.88	19.64	437.79		207.10			0.44
14.00	ML	3.13	19.64	437.79		231.72			0.44
15.00	ML	0.12	19.64	437.79		247.70			0.44

Table 3.- Soil model considered for BH-03

Layer	Type	Thickness	ϒ	V_s	IP	σ'_{vo}	S_u	OCR	k_0
1.00	Fill	1.00	19.00	177.82		9.50	66.05		1.00
2.00	CH	2.09	15.00	177.82	50.00	34.67	66.05	8.92	0.65
3.00	CH	0.71	15.00	177.82	40.00	55.68	66.05	4.54	0.61
4.00	ML	1.97	15.00	177.82		66.11		0.00	0.44
5.00	ML	1.85	15.00	177.82		76.02		0.00	0.44
6.00	MH	1.91	14.00	138.83	65.00	84.82	47.52	1.56	0.71
7.00	MH	1.54	14.00	138.83	42.00	92.05	47.52	1.39	0.62
8.00	MH	1.91	14.00	138.83	39.00	99.28	47.52	1.25	0.60
9.00	MH	1.47	14.00	138.83	37.00	106.36	47.52	1.13	0.60
10.00	MH	2.60	15.00	138.83	47.00	116.19	47.52	1.00	0.64
11.00	MH	2.38	15.00	138.83	43.00	129.11	47.52	0.86	0.62
12.00	MH	4.61	15.00	151.96	49.00	147.25	53.59	0.84	0.65
13.00	MH	8.01	15.00	151.96	43.00	180.00	53.59	0.63	0.62
14.00	ML	2.00	15.00	330.58		205.97			0.44
15.00	SC	1.53	15.00	330.58		215.13			0.44

Table 4.- Soil model considered for BH-01

Layer	Type	Thickness	ϒ	V_s	IP	σ'_{vo}	S_u	OCR	k_0
1.00	Fill	0.71	19.00	117.05		6.75	37.87		1.00
2.00	CH	2.84	16.00	117.05	36.00	36.21	37.87	3.80	0.59
3.00	ML	0.25	16.00	117.05		60.93			0.44
4.00	ML	2.25	16.00	117.05		69.89			0.44
5.00	SM	0.71	16.00	117.05		79.05			0.44
6.00	ML	0.71	16.00	117.05		83.44			0.44
7.00	SM	0.71	16.00	117.05		87.84			0.44
8.00	ML	0.71	16.00	117.05		92.23			0.44
9.00	ML	2.14	17.00	190.95		102.13			0.44
10.00	SM	1.43	17.00	190.95		114.96			0.44
11.00	MH	2.85	16.00	190.95	21.00	128.92	72.61	1.57	0.53
12.00	MH	15.00	16.00	127.94	43.00	184.17	42.63	0.44	0.62
13.00	MH	4.28	16.00	271.73	28.00	243.84	116.08	1.24	0.56

Table 5.- Soil model considered for BH-02